Publication History
Submitted: 8th May 2017
Accepted: 13th June 2017
Published Online: 19th June 2017

Manuscript submitted to European Journal of Pharmaceutical Sciences

# Development of MPC-DPA polymeric nanoparticle systems for inhalation drug delivery applications

Abdul Khaliq Elzhry Elyafi[1], Guy Standen[1], Steven T. Meikle[1], Andrew L. Lewis[2], Jonathan P. Salvage[1]*

[1]University of Brighton, School of Pharmacy and Biomolecular Sciences, Huxley Building, Lewes Road, Brighton, BN2 4GJ, UK.

[2]Biocompatibles UK Ltd, BTG International Group Company, Lakeview, Riverside Way, Watchmoor Park, Camberley, GU15 3YL, UK.

*Corresponding Author
Dr Jonathan P. Salvage
University of Brighton
School of Pharmacy and Biomolecular Sciences
Huxley Building,
Lewes Road,
Brighton, BN2 4GJ
UK.
E-mail: J.P.Salvage@brighton.ac.uk

**Abstract**

Inhalation of nanoparticles for pulmonary drug delivery offers the potential to harness nanomedicine formulations of emerging therapeutics, such as curcumin, for treatment of lung cancer. Biocompatible nanoparticles composed of poly(2-methacryloyloxyethyl phosphorylcholine)-*b*-poly(2-(diisopropylamino)ethyl methacrylate) (MPC-DPA) have been shown to be suitable nanocarriers for drugs, whilst N-trimethyl chitosan chloride (TMC) coating of nanoparticles has been reported to further enhance their cellular delivery efficacy; the combination of the two has not been previously investigated. Development of effective systems requires the predictable, controllable, and reproducible ability to prepare nanosystems possessing particle sizes, and drug loading capacities, appropriate for successful airway travel, lung tissue penetration, and tumour suppression. Although a number of MPC-DPA based nanosystems have been described, a complete understanding of parameters controlling nanoparticle formation, size, and morphology has not been reported; in particular the effects of differing solvents phases remains unclear. In this current study a matrix of 31 solvent combinations were examined to provide novel data pertaining to the formation of MPC-DPA nanoparticles, and in doing so afforded the selection of systems with particle sizes appropriate for pulmonary delivery applications to be loaded with curcumin, and coated with TMC. This paper presents the first report of novel data detailing the successful preparation, characterisation, and optimisation of MPC-DPA nanoparticles of circa 150 – 180 nm diameter, with low polydispersity, and a curcumin loading range of circa 2.5 – 115 μM, tunable by preparation parameters, with and without TMC coating, and thus considered suitable candidates for inhalation drug delivery applications.

**Keywords:**

MPC-DPA; Nanoparticles; Curcumin; TMC; Inhalation; Pulmonary drug delivery.

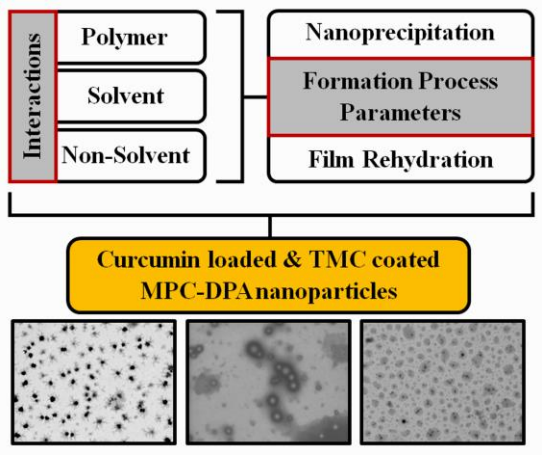

## 1. Introduction

The pulmonary route for therapeutic administration, via inhalation, is a well-suited and effective way to deliver therapeutic forms of hormones, peptides, and other drug molecules which are not easily absorbed through the gastrointestinal tract, into systemic circulation (Barnett, 2004; Kuzmov and Minko, 2015; Mack, 2007). Additionally, recent studies have highlighted that pulmonary delivery can be an effective method for the treatment of lung cancer, compared to the limitations associated with of conventional treatments such as chemo and radio therapy (Minko et al., 2013).

The phosphorylcholine (PC) containing copolymer poly(2-methacryloyloxyethyl phosphorylcholine)-*b*-poly(2-(diisopropylamino)ethyl methacrylate) (MPC-DPA) has well proven biocompatibility (Giacomelli et al., 2006; Porto et al., 2011; Yallapu et al., 2010; Yoshikawa et al., 2011), and self-assembles to form a range of nanostructures, including micelles, polymersomes, and higher-order assemblies when the DPA block is deprotonated at physiological pH 7.4. (Blanazs et al., 2009; Derry et al., 2016; Du et al., 2005; Pearson et al., 2013; Porto et al., 2011; Robertson et al., 2014). Moreover, when subsequently exposed to an acidic environment, for example tumor tissue, the DPA becomes protonated and hydrophilic, and the nanoparticles disassemble releasing the therapeutic payload (Pearson et al., 2013; Pegoraro et al., 2013; Salvage et al., 2005). Previous studies have highlighted that MPC-DPA diblock copolymers have the potential to be applied to a range of nanoparticle based clinical therapies, which can utilise the stable nanoparticles for drug delivery and cell targeting of hydrophobic and hydrophilic molecules, proteins, antibodies, and also genetic material (Canton et al., 2013; Colley et al., 2014; Licciardi et al., 2008, 2006, 2005, Lomas et al., 2010, 2008, 2007, Mu et al., 2008; Pegoraro et al., 2014, 2013; Salvage et al., 2005, 2015, 2016). However, copolymer size, the molecular weight (Mw), can affect membrane properties of the nano-assemblies, including thickness, rigidity, stability, and the mechanical properties of the resultant morphology formed (Ahmed et al., 2006; Discher et al., 2007; Discher and Ahmed, 2006; Motornov et al., 2010). Additionally, the stability and morphology of MPC-DPA nanoparticles depends on several key factors including the formation process, copolymer concentration, and the solvents used during assembly (Pearson et al., 2013; Pegoraro et al., 2014; Salvage et al., 2015). The predominant processes reported for the formation of MPC-DPA nanoparticles have been nanoprecipitation (Salvage et al., 2015, 2016) and film rehydration (Canton et al., 2013; Colley et al., 2014; Robertson et al., 2014), both of which use solvents within the process. However, there appears to be no single solvent combination suitable to dissolve the different block length copolymers at the same concentration (Ye et al., 2015). It has also been reported previously that MPC-DPA copolymers are selectively soluble in some organic solvents (Edmondson et al., 2010; Licciardi et al.,

2005; Porto et al., 2011), and that choice of solvent can influence the resultant self-assembled nanoparticle size and polydispersity (Alexandridis and Spontak, 1999; Israelachvili, 2011; Meyer et al., 2006; Salvage et al., 2015); however, to date, there has been no detailed and focused study of this effect

Curcumin is an active pharmaceutical ingredient (API) which has demonstrated anti-cancer effects against lung, ovarian, pancreatic and colorectal cancers (Gou et al., 2011; Mock et al., 2015; Patil et al., 2015). However, the therapeutic advantages are often attenuated after oral administration due to the physicochemical properties of curcumin, such as low water solubility, < 1µg/mL, and a rapid half-life, with poor systemic bioavailability of < 1 %. (Betbeder et al., 2015; Nahar et al., 2015; Patil et al., 2015; Shanmugam et al., 2015; Tomren et al., 2007; Xie et al., 2011; Zhang et al., 2013). To overcome these limitation, a number of approaches have been investigated previously, such as solid dispersions (Paradkar et al., 2004), liposomes (Saengkrit et al., 2014), and polymeric micro and nanoparticles (Kakran et al., 2012; Zhang et al., 2013), although none of these approaches yielded significant improvements in bioavilability.

N-trimethyl chitosan chloride (TMC), like chitosan, has mucoadhesive properties which can help increase the transit time of drug nano-carriers into the gastrointestinal tract (GIT) and the absorption rate of drugs (Amidi et al., 2006; Zhang et al., 2013). Additionally, TMC can increase paracellular diffusion of nanoparticles, and drugs including curcumin, via epithelial cells by opening the tight junctions of the cell membrane (Amidi et al., 2006; El-Sherbiny and El-Baz, 2015; Guan et al., 2012; Sahni et al., 2008; Steed et al., 2010; Zhang et al., 2013). Compared to chitosan, TMC is more soluble in aqueous solutions, especially at neutral physiological pH 7.4 (Sahni et al., 2008). It also has the ability to improve formulation stability and bioavailability, the stability of liposomes after coating, and is an effective enhancer of hydrophilic drug and protein absorption (Chen et al., 2016; Panya et al., 2010). Moreover, TMC has displayed strong electrostatic interactions between polymer cationic amine groups and negatively charged tumor cells, thus providing targeted drug delivery properties (Guan et al., 2012; Thanou et al., 2000). Indeed, TMC has been shown to have many promising micro and nanoparticle based applications for oral, nasal, pulmonary, ocular, and intestinal delivery of drugs (Amidi et al., 2006; El-Sherbiny and El-Baz, 2015; Guan et al., 2012; Sahni et al., 2008). Thus TMC coating of MPC-DPA nanoparticles may enhance their efficacy further, and contribute towards developing curcumin formulations with potential clinical applications for pulmonary delivered treatment of human lung cancers (Basnet and Skalko-Basnet, 2011; Gou et al., 2011; Kakran et al., 2012; Mock et al., 2015; Nahar et al., 2015; Patil et al., 2015; Prasad et al., 2014; Saengkrit et al., 2014; Wang et al., 2015).

The study reported herein investigated the development of MPC-DPA nanoparticles as potential pulmonary drug delivery vehicles, based on controlling particle size such that effective airway travel and lung tissue penetration would theoretically be achievable. Preparation and characterisation was undertaken using two contrasting nanoparticle formation methods, nanoprecipitation and film rehydration, and the effects of 31 solvent mixes on nanoparticle size and polydispersity studied. After this initial screening, nanoparticle formulations possessing particle size and polydispersity values reported as suitable for pulmonary route applications, were selected for subsequent curcumin drug loading, which has promising anticancer effects, and TMC surface modification, which has tissue penetration enhancing properties. In summary, this paper details for the first time novel data pertaining to the development of curcumin loaded, and TMC modified, MPC-DPA nanoparticle formulations for inhalation based lung cancer therapies, and has also provided an extensive matrix of novel particle size controllability data that will be of value for development of further novel MPC-DPA nanoparticle based pharmaceutical delivery applications.

## 2. Methods and materials

### *2.1. Materials*

The $MPC_{30}$-$DPA_{100}$ and $MPC_{100}$-$DPA_{100}$ block copolymers were supplied by Prof Steven Armes (University of Sheffield, UK) having been synthesised by atom transfer radical polymerisation (ATRP), as detailed previously (Ma et al., 2003; Salvage et al., 2005). Methanol, ethanol, chloroform, isopropanol, acetonitrile, phosphate buffered saline, phosphotungstic acid, hydrochloric acid, sodium hydroxide, sodium chloride, deuterium oxide, curcumin 98%, methyl iodide 99%, sodium iodide 99%, 1-methyl-2-pyrrolidone 99.5%, 2 mL glass vials, 20 mL glass vials, 13 mm diameter glass cover slips, 2 mL plastic syringes, 0.45 µm and 0.22 µm syringe filters, were purchased from Fisher Scientific, UK. Transmission electron microscopy (TEM) grids were purchased from Agar Scientific, UK. Chitosan (200 - 400 kDa) was purchased from Sigma-Aldrich, UK. Atomic force microscopy (AFM) cantilever tips were purchased from Windsor Scientific, UK.

### *2.2. NMR and GPC characterisation*

Block ratio composition and molecular weight of the received MPC-DPA block copolymers was confirmed using $^{1}H$ nuclear magnetic resonance (NMR) spectroscopy and gel permeation chromatography (GPC) using methods detailed previously (Salvage et al., 2016).

*2.3. Solvent solubility*

The solubility of the MPC-DPA copolymers in organic solvents of differing polarity values (Table 1) was assessed for a matrix of 31 solvent combinations utilising methanol, ethanol, chloroform, isopropanol, and acetonitrile, as shown in Table 2. For each solvent combination, copolymer solutions were prepared (40 mg/mL) and allowed to equilibrate for two days, at room temperate, for dissolution to complete. The copolymer solutions were then visually assessed, and solubility in each of the 31 solvents designated as one of three British Pharmacopeia based solubility classes: completely soluble, slightly soluble, and practically insoluble.

*2.4. Nanoprecipitation formation of nanoparticle systems*

Copolymer solutions (40 mg/mL) in the 31 solvents (Table 2) were prepared for $MPC_{30}$-$DPA_{100}$ and $MPC_{100}$-$DPA_{100}$. The nanoprecipitation process was adapted from a published method (Salvage et al., 2015), whereby aliquots (100 µL) of the copolymer solutions were added drop-wise to 10 mL of phosphate buffer saline (PBS) (pH 7.4) and stirred (600 rpm) for 4 minutes with a magnetic stir bar (20 mm) to facilitate solvent evaporation. Copolymer concentration of the prepared nanoparticle systems was 0.4 mg/mL. Independent (n = 3) triplicate repeats of the experimental work were undertaken.

*2.5. Film-rehydration formation of nanoparticle systems*

Copolymer solutions (5 mg/mL) in 6 solvents selected from the 31 solvent matrix (Table 2), based on the nanoprecipitation data, were prepared for $MPC_{30}$-$DPA_{100}$ and $MPC_{100}$-$DPA_{100}$. Aliquots (10 mL) of these were added to 20 mL glass vials, and the solvent removed via evaporation in a Fistreem digital vacuum oven (1000 mbar) at 50 °C for 8 hours. The copolymer films in the glass vials were then rehydrated using 10 mL of PBS (pH 7.4) with constant stirring (200 rpm), via a magnetic stir bar (15 mm), for 1 week at ambient room temperature, and then sonicated for 15 minutes to reduce the average particle size and polydispersity (Battaglia et al., 2011; Pegoraro et al., 2014; Sorrell et al., 2014). The resultant samples (5 mg/mL) were further diluted with PBS (pH 7.4) to provide 0.5 mg/mL copolymer nanoparticle systems. Independent (n = 3) triplicate repeats of the experimental work were undertaken.

*2.6. Nanoparticle system characterisation*

The prepared MPC-DPA nanoparticle systems were assessed for particle size, polydispersity, zeta potential, and particle morphology, using dynamic light scattering (DLS), laser Doppler electrophoresis (LDE), and scanning transmission electron microscopy (STEM).

*2.6.1 Dynamic light scattering*

Particle size (*ZAve*) and polydispersity (Pd) of the nanoparticle systems were measured in triplicate at 25° C, with a Malvern Zetasizer Nano ZS90 instrument, using the DLS method detailed previously (Salvage et al., 2016). Samples were examined unfiltered, syringe filtered 0.45 µm, and syringe filtered 0.22 µm. The particle size data are presented as intensity based hydrodynamic diameters ($D_h$), with average nanoparticle system particle size (*ZAve*) determined via Cummulants analysis, and where multiple particle population peaks were present within a sample, individual peak average diameters ($D_h^1$, $D_h^2$, $D_h^3$) determined by non-negative least square (NNLS) analysis. Independent (n = 3) triplicate repeats of the experimental work were undertaken.

*2.6.2. Laser Doppler electrophoresis*

Zeta potential of the nanoparticles was determined via LDE, using a Malvern Zetasizer Nano ZS90 instrument at 25 °C, with Malvern DTS 1061 capillary cells and DTS 1235 zetapotential standards. Data consisted of the average value of three consecutive, 120 seconds, measurements, composed of 12 runs. The LDE technique measured the electrophoretic mobility of the nanoparticles, and then used the Henry equation ($U_E = 2\varepsilon\, z\, f(Ka) / 3\eta$), where $U_E$ = electrophoretic mobility, ε = dielectric constant, $z$ = zetapotential, $f(Ka)$ = Henry's function, and η = viscosity, to calculate the zeta potential. Independent (n = 3) triplicate repeats of the experimental work were undertaken.

*2.6.3. Scanning transmission electron microscopy*

Particle morphology was investigated via STEM, using a Zeiss SIGMA field emission gun scanning electron microscope (FEG-SEM) equipped with a Zeiss STEM detector. Working conditions used were; 20 kV accelerating voltage, 20 µm aperture, and 3 mm working distance. To prepare the STEM samples, 200 mesh Formvar coated copper TEM grids were plasma treated, 40 seconds at 5 watts, in a Polaron PT7150 plasma barrel etcher for 30 seconds, to improve surface wettability. Then 1 drop of sample (0.22 µm filtered) was applied to the TEM grid for 60 seconds, excess wicked way, 1 drop of filtered (0.22 µm) 2% phophotungstic

acid (PTA) (pH 7.4) applied to the TEM grid for 60 seconds, excess wicked away, and then air dried at room temperature.

*2.7. Atomic force microscopy*

Copolymer film morphology and roughness were examined via AFM, using a Digital Instruments Dimension D3000 AFM, equipped with a Nanoscope 111A controller. The AFM was operated in tapping mode, at a scan rate of 0.25 Hz, a scan size of 100 µm, and using Nanosensor PointProbe NCH-W cantilever AFM tips. The copolymer films (5 mg/mL) were prepared by applying 1 drop of copolymer-solvent sample to a 13 mm diameter glass coverslip.

*2.8. TMC synthesis*

The N-trimethyl chitosan chloride (TMC) synthesis was undertaken via nucleophilic substitution using methyl iodide in a two-step reaction to produce a high degree of quarterisation (DQ %) in accordance with published protocols (Patrulea et al., 2015; Sahni et al., 2008; Sieval et al., 1998). The chitosan degree of deacetylation (DDA) (Lavertu et al., 2003), and the TMC degree of quaternisation (DQ) (Patrulea et al., 2015; Thanou et al., 2000), were determined by $^{1}$H NMR in deuterium oxide ($D_2O$) using a 400 MHz Bruker Ascend spectrometer and were calculated according to equations 1 and 2, respectively:

$$\text{DDA (\%)} = \left(\frac{H1D}{H1D + HAc/3}\right) \times 100 \quad \ldots\ldots\ldots\ldots\ldots\ldots (1)$$

Where: H1D is the value of the integral for the peak of proton H1 of deacetylation monomer at chemical shift 5.211 ppm; and HAc is the peak of the three protons of acetyl group at chemical shift 2.351 ppm.

$$\text{DQ (\%)} = \left(\frac{[(CH3)3]}{[H]} \times \frac{1}{9}\right) \times 100 \quad \ldots\ldots\ldots\ldots\ldots\ldots (2)$$

Where: [(CH3)3] is the value of the integral for the peak of trimethyl amino function [-N+(CH3)3] at chemical shift 3.3 ppm; and the [H] is the value of the integral for the peaks of the proton H1 of chitosan at chemical shift 4.7 and 5.4 ppm and used as internal standards.

*2.9. Calibration curves for curcumin solubility and loading*

To determine the solubility of curcumin in the solvents (ethanol-isopropanol and methanol-ethanol-chloroform-acetonitrile) used for nanoparticle loading (Section 2.10), standard curves were constructed using a PerkinElmer

Lambda 25 UV-Vis spectrophotometer. Curcumin in solvent solutions were prepared (0 – 12 mg/L), the λ max measured, the absorbance of the dilutions recorded at the λ max, and the standard curves plotted. Saturated solutions of curcumin in solvent were then prepared (Baka et al., 2008), filtered (0.22 μm) to remove undissolved curcumin, diluted to the linear range, the absorbance at λ max measured, and the curcumin solubility calculated from the standard curves.

To determine curcumin encapsulation and loading efficiency, standard curves were also prepared for curcumin at pH 1.6 in PBS-methanol (1:9 v/v), as curcumin has been shown to degrade in alkaline conditions (Liu et al., 2012; Wang et al., 1997), and has greater stability in acidic solutions (Tomren et al., 2007). Aliquots (1 mL) of the curcumin loaded MPC-DPA nanoparticle in PBS formulations (Section 2.10), were then dissolved in 9 mL of methanol (pH 1.6), diluted to the linear range, the absorbance at λ max measured, the curcumin content determined from the standard curve, and the encapsulation efficiency and loading capacity calculated from equations 3 and 4. Independent (n = 3) triplicate repeats of the experimental work were undertaken.

$$\text{Encapsulation efficiency (EE\%)} = \left[\frac{\text{weight of curcumin in nanoparticles}}{\text{weight of feed curcumin}}\right] \times 100 \quad \text{…….....(3)}$$

$$\text{Loading capacity (LC\%)} = \left[\frac{\text{weight of curcumin in nanoparticles}}{\text{weight of feed copolymer}}\right] \times 100 \quad \text{…….....(4)}$$

*2.10. Curcumin loaded nanoparticle systems*

MPC-DPA nanoparticle systems loaded with curcumin were prepared for formulation 12 ($MPC_{100}$-$DPA_{100}$ in ethanol-isopropanol) and formulation 26 ($MPC_{30}$-$DPA_{100}$ in methanol-ethanol-chloroform-acetonitrile) as per the nanoprecipitation (Section 2.4) and film-rehydration (Section 2.5) samples, using curcumin saturated solvents. The solubility of curcumin in the solvents used, and the curcumin encapsulation efficiency and loading capacity of the prepared MPC-DPA nanosystems were determined using standard curves as per Section 2.9. Independent (n = 3) triplicate repeats of the experimental work were undertaken.

*2.11. TMC coated MPC-DPA nanoparticles*

Coating of the MPC-DPA curcumin loaded nanoparticle systems with TMC polymer was undertaken by firstly preparing samples as per Section 2.10. TMC was then added to the samples at 1 mg/mL with stirring (200 rpm) for 24 hours to coat the nanoparticles. The TMC coated nanoparticle systems were characterised using the

methods described in Sections 2.6 and 2.9, for particle size and polydispersity, zetapotential, morphology, and curcumin encapsulation efficiency and loading capacity. Independent (n = 3) triplicate repeats of the experimental work were undertaken.

*2.12. Fourier transform infrared spectroscopy*

To investigate the chemical structure of curcumin, potential interactions between curcumin and the MPC-DPA copolymers, the structure of MPC-DPA copolymers, chitosan, and the synthesised TMC polymers, Fourier transform infrared spectroscopy (FTIR) was performed using a PerkinElmer Spectrum 65 FT-IR Spectrometer. All transmission spectra were obtained at ambient temperature by recording the average of 32 scans in the region between a wave number 4000 and 650 $cm^{-1}$ with a resolution of 4 $cm^{-1}$.

## 3. Results and Discussion

*3.1. NMR and GPC characterisation*

The composition of the $MPC_{30}$-$DPA_{100}$ and $MPC_{100}$-$DPA_{100}$ diblock copolymers, confirmed via $^{1}H$ NMR and GPC, and shown in Fig. 1a and 1b respectively, and Table 3, was consistent with previous reports (Ma et al., 2003; Salvage et al., 2005), indicating good control of polymer synthesis and stability.

*3.2. Solvent solubility*

To explore the influence of organic solvent properties, polarity and miscibility in water, upon the formation of nanoparticles, and the properties of particle size and polydispersity, a matrix comprising 31 organic solvent combinations containing $MPC_{30}$-$DPA_{100}$ and $MPC_{100}$-$DPA_{100}$ copolymers (40 mg/mL) were prepared. The resultant copolymer solutions were visually classified for solubility in Table 4. The polarity value of the solvents indicated the expected level of polymer solvent interaction, and will also have influenced the contact force, surface tension, between the MPC-DPA copolymer and solvents, thus influencing the resultant aggregate structure and homogeneity of the bulk solution (Ye et al., 2015). The data suggested that $MPC_{100}$-$DPA_{100}$ copolymer was more soluble in the 31 solvent combinations than $MPC_{30}$-$DPA_{100}$, possibly due to the higher ratio of amphiphilic block copolymer MPC, and thus more hydrophilic nature.

*3.3. Nanoprecipitation formation of nanoparticle systems*

For $MPC_{30}$-$DPA_{100}$ nanoparticles in PBS (pH 7.4), formed via nanoprecipitation from the 31 solvent combinations, DLS analysis revealed a wide range of average particle sizes (*ZAve*) and polydispersity (Pd) values, as seen in Table 5. The particle sizes produced were consistent with those of micelles, polymersomes, and high-order assemblies (Du et al., 2005; Pearson et al., 2013). Exceptions were formulations 3, 4, 13 and 14 which did not produce measurable nanoparticles, which correlated with the solvent solubility data (Table 4), indicating polymer insolubility in those solvent combinations. Additionally, formulations 10, 17, 19, and 25 resulted in loss of nanoparticle presence upon filtration, principally due to exclusion of large particle aggregates. Similar observation was noted for $MPC_{100}$-$DPA_{100}$ nanoparticle systems, except for formulations 3, 4 and 13 as seen in Table 5, however there were no filtration associated total particle losses, possibly due to the more hydrophilic nature of the $MPC_{100}$ block relative to the $MPC_{30}$ block. Regarding the filtration process, using 0.45 and 0.22 μm filters, the average particle size and polydispersity of the MPC-DPA nanoparticles was reduced upon passing through the filter, which was in agreement with previous work (Salvage et al., 2015, 2016). Without filtration $MPC_{30}$-$DPA_{100}$ nanoparticles displayed larger mean particle sizes compared to $MPC_{100}$-$DPA_{100}$ nanoparticles. However, after filtration (0.22 μm), $MPC_{100}$-$DPA_{100}$ produced larger nanoparticles with a higher polydispersity compared to $MPC_{30}$-$DPA_{100}$. These results were not unexpected, as the $MPC_{100}$-$DPA_{100}$ copolymer structure has a higher degree of amphiphilic MPC block polymer compared to $MPC_{30}$-$DPA_{100}$, and the findings were in agreement with previous reports of degree of polymerisation influencing particle size and morphology when using the same organic phase (Patikarnmonthon, 2013). In summary, these data indicated that particle size was dependent upon the type and nature of organic solvent combination used, could be refined with filtration, and was in agreement with previous reports of solvent choice effects (Bilati et al., 2005; Salvage et al., 2015).

In order to select suitable comparators against the film rehydration process, assessment of the post-filtration (0.22 μm) data, (Table 5 and Table 6), indicated that nanoprecipitation formulations 15, 24, 26 for $MPC_{30}$-$DPA_{100}$, and 12, 16, 29 for $MPC_{100}$-$DPA_{100,}$ had the largest mean particle sizes combined with the lowest polydispersity values, and were thus chosen.

### *3.4. Film-rehydration formation of nanoparticle systems*

The MPC-DPA film rehydration samples for solvent combinations 15, 24, 26, ($MPC_{30}$-$DPA_{100}$) and 12, 16, 29 ($MPC_{100}$-$DPA_{100}$) were formed via solvent casting of the polymer film, followed by rehydration in PBS (pH 7.4), with stirring, over a 7 day period. It can be seen from Figure 2 that there were visible differences in the rate of

film rehydration and polymer solubilisation between the polymers. Immediately after addition of the PBS (t = 0) $MPC_{100}$-$DPA_{100}$ polymer films began to hydrate, whilst the less hydrophilic $MPC_{30}$-$DPA_{100}$ did not (Figure 2a). This slower rate of rehydration was evident for $MPC_{30}$-$DPA_{100}$ throughout the subsequent experimental time course (Figure 2b-d), until apparent full rehydration was reached at day 7 (t = 7) (Figure 2e). There was also visual evidence suggesting that the solvent used for casting influenced rate of film rehydration. To investigate this further, AFM analysis of the polymer films was undertaken.

The AFM data indicated that the film structure and surface morphology, of the copolymer films, were different when using the selected solvent combinations, between and within the two copolymers, as shown in Table 7 and Figure 3. In addition, it was evident that the surface roughness measurement data was greater for formulations 12, 15, 24 and 29 (Table 7), which contained isopropanol, but no chloroform, relative to formulations 16 and 26, which contained chloroform, but no isopropanol. As seen in Table 1, Isopropanol had a higher viscosity and boiling point than chloroform, and these data illustrated that solvent properties can influence copolymer conformations when drying, and affect the resultant copolymer film topology. Furthermore, the higher level of film surface roughness can lead to greater adhesive strength of the copolymer films (Bowen et al., 1998) , and therefore rehydration of the film, and creation MPC-DPA nanoparticles, may require an increased stirring shear rate or time, as seen in Figure 2.

Following the 7 day film rehydration, samples underwent sonication for 15 mins to reduce the heterogeneous morphology of nanoparticles in the systems (Yealland, 2015), followed by DLS particle size measurement and STEM imaging of the nanoparticles. As seen with the nanoprecipitation samples, $MPC_{30}$-$DPA_{100}$ nanoparticles formed by film rehydration possessed larger average particle sizes, compared to the $MPC_{100}$-$DPA_{100}$, without filtration as shown in Table 8. This may have been due to the hydrophobic effect of $DPA_{100}$ in the copolymer being stronger than the amphiphilic effect of $MPC_{30}$, and thus consistent with the slower hydration observed (Figure 2) and resultant larger diameter nano-assemblies. However, when samples were filtered (0.45 and 0.22 µm), the particle sizes and polydispersity values were greatly reduced for both $MPC_{30}$-$DPA_{100}$ and $MPC_{100}$-$DPA_{100}$ samples, resulting in average diameters in the 120 – 150 nm size range, which was consistent with MPC-DPA polymersome sizes (Du et al., 2005).

In summary, the DLS data (Table 8), indicated that filtration (0.22 µm) of MPC-DPA film rehydration samples offers the potential to controllably produce nanoparticles of low polydispersity, with good reproducibility, and the size viewed a suitable for inhalation delivery applications with maximum therapeutic efficacy (Cipolla et al.,

2013; Garbuzenko et al., 2014; Gratton et al., 2008; Hu et al., 2014; Koshkina et al., 2001; Kuzmov and Minko, 2015; Ungaro et al., 2012).

*3.5. Comparison of nanoprecipitation vs film rehydration*

The methods used to create MPC-DPA nanoparticles, with or without drug loading, were nanoprecipitation and film rehydration, as described earlier, which have specific properties and requirements associated with each (Battaglia and Ryan, 2006; Messager et al., 2014). For example, the nanoprecipitation method is a bottom-up procedure which assembles nanoparticles from copolymer molecules via the rapid injection of dissolved copolymer organic phase into an aqueous phase. Due to using free moving molecules, this method is a fast production procedure, capable of reproducibly forming nanoparticles of low polydispersity. In contrast, the film rehydration method is a top-down approach, and depends upon transition of the bulk copolymer molecules from dried, cast film, state, through a copolymer swelling phase, to formation of dispersed polymer nanoparticles, which are primarily polymersomes. These often display, large, micron, particle scale, and require mechanical energy input to form, such as high shearing and stirring rates, and sonication. This method has some disadvantages, for example a long processing and formation time, high energy input, and in some cases is not suitable for encapsulation of heat sensitive drugs (Bilati et al., 2005; Messager et al., 2014; Sadeghi et al., 2016; Schubert and Muller-Goymann, 2003)

In this current study, the nanoprecipitation data and film-rehydration data suggest that there were apparent differences in the size and polydispersity of the nanoparticles formed via the contrasting methods. Thus, when these parameters were compared for the $MPC_{30}$-$DPA_{100}$ formulations 15, 24, 26, and the $MPC_{100}$-$DPA_{100}$ formulations 12, 16, 29, that had been prepared via the two methods, there were indeed clear particle size and polydispersity shifts evident, as shown in Figures 4a, 4b, and 4c. The more hydrophobic nature of $MPC_{30}$-$DPA_{100}$ initially lead to the formation of larger nanoparticles, as the hydrophobicity can impede particle aggregation in aqueous solutions (Bilati et al., 2005). However, following the 0.22 μm filtration process, the $MPC_{100}$-$DPA_{100}$ nanoparticles also displayed a larger nanoparticle size, possibly due to a thicker outer corona on the particles resulting from the MPC block length, with $MPC_{100}$ being longer than $MPC_{30}$ (Giacomelli et al., 2006; Salvage et al., 2005).

Additionally, when the two methods of nanoparticle formation without filtration were compared, the film rehydration method resulted in the formation of larger nanoparticles, with lower reproducibility, as seen in

Figure 4a, and also increased solution turbidity. This may have been the result of the copolymer concentration being 5 mg/mL for film rehydration, in contrast to the lower 0.4 mg/mL concentration used for nanoprecipitation. These results were consistent with Bilati et al. (2005) and Salvage et al. (2015, 2016) in that they displayed an increase in the particle size, when polymer concentration was increased. To determine the morphology of the nanoparticles formed, and establish the presence of either micelles or polymersomes, the $MPC_{30}$-$DPA_{100}$ formulations (15, 24, 26) and $MPC_{100}$-$DPA_{100}$ formulations (12, 16, 29) prepared by the two methods employed, nanoprecipitation and film-rehydration, were examined using STEM. As seen in Figures 5 and 6, both copolymers were successful in forming nanoparticles in the two formation processes. For the nanoprecipitation samples, (Figure 5), STEM analysis indicated that these consisted predominately of small unilamellar vesicles with a spherical morphology and size consistent with polymersomes. However, for the film rehydration samples, a mixture of particle morphologies were observed, with polymersome sized nanoparticles present, as evidenced by the DLS data (Figure 4c), together with larger polymer aggregates with irregular structures and elongated edges, as shown in Figure 6. This was consistent with previous reports of film rehydration particle population complexity (Robertson et al., 2016), where exploration and purification of film rehydration particle populations was undertaken. The STEM data was largely consistent with the DLS data, in that there was a visible difference in nanoparticle size between all formulations due to the different methods of formation, and the copolymer compositions. Furthermore, the STEM images (Figures 5 and 6) suggested that nanoprecipitation was more effective at forming a homogeneous population of polymersomes, compared with film rehydration. This was possibly due to the copolymer being molecularly dissolved in the organic phase immediately prior to nanoprecipitation, therefore the forces holding the copolymer chains together were weaker (Ye et al., 2015) and thus allowed rapid nanoparticle formation. It appeared from Figure 9 that $MPC_{100}$-$DPA_{100}$ formed polymer aggregates with thicker particle coronas than $MPC_{30}$-$DPA_{100}$, which may have been the result of $MPC_{100}$-$DPA_{100}$ having a higher degree of polymerisation MPC block (Du et al., 2005). The morphology of MPC-DPA polymersomes, as well as aggregation style, can be influenced by several factors, including, the formation process, nature of organic solvents used, the hydrophobic to hydrophilic balance of copolymer blocks, polymer concentration, and stirring speed and duration (Ayen et al., 2011). According to the DLS data (Figures 4a, 4b, and 4c) and STEM images (Figures 5 and 6) for characterisation of the MPC-DPA nanoparticles, the formulations 12 and 26, for both $MPC_{100}$-$DPA_{100}$ and $MPC_{30}$-$DPA_{100}$, possessed a large particle size together with low polydispersity, and spherical morphology, and were therefore selected for subsequent curcumin loading.

In summary, the solvent, non-solvent, and ratio used, together with copolymer composition, can affect the resultant nanoparticle size and morphology. Additionally, STEM data (Figures 5 and 6) suggested that, in this instance, nanoprecipitation was more effective at forming homogeneous populations of vesicle morphology nanoparticles, polymersomes, than the film rehydration method which requires subsequent particle fractionation and purification before use (Robertson et al 2016).

*3.6. TMC synthesis*

The physicochemical properties of chitosan can be affected by the degree of deacetylation, and the percentage of deacetylated and acetylated monomer plays an important role in TMC synthesis efficacy. Therefore, before TMC synthesis was undertaken, the degree of deacetylation (DDA%) of chitosan was calculated (Lavertu et al., 2003). The $^{1}$H NMR spectrum of the chitosan polymer (Figure 7a), which consisted of acetylated and deacetylated monomers, was consistent with previously reported spectra (Lavertu et al., 2003). As such, the chemical shift at 2.351 ppm was attributed to the three protons of acetyl group (-CO-$CH_3$) in acetyl units (H-Ac), while the chemical shifts at 4.918 and 5.211 ppm were assigned to protons H1 for both acetylated (H1-A) and deacetylated (H1-D) units. Additionally, the chemical shifts between 3.916 and 4.225 ppm corresponded to protons H2, H3, H4, H5, and H6 (H2-6) of glycosidic ring of chitosan, the chemical shift at 3.518 ppm was assigned to proton H2 in deacetylated units, and the shift at 4.733 ppm belonged to the solvent (HOD) proton (Lavertu et al., 2003). According to the proposed shift assignments within the NMR spectra (Figure 7a) and the equation (1), the degree of deacetylation (DDA) of chitosan used for TMC synthesis was 81%.

The TMC was synthesized from high molecular weight chitosan using the two step method (Polnok et al., 2004; Sahni et al., 2008; Sieval et al., 1998) the resultant polymer was a white powder, which was soluble in water, the $^{1}$H NMR spectra for the TMC is shown in Figure 7b. The chemical shifts at 2.55, 3.05, and 3.8 ppm were assigned to $–NHCH_3$, $-N(CH_3)_2$ and $–N^{+}(CH_3)_3$ groups from the TMC structure, respectively, and was consistent with previous reports (Hansson et al., 2012; Patrulea et al., 2016; Sieval et al., 1998). Additionally, the chemical shifts at 4.8 and 5.25 ppm that were assigned to the H1 proton of chitosan and its derivatives, as described in previous reports (Hansson et al., 2012; Patrulea et al., 2015; Thanou et al., 2000), had disappeared. According to the proposed shift assignments, and using the equation (2), the degree of quaternization (DQ) of TMC after the two step synthesis was high, at 75%, and this result corresponded well with other reports (Patrulea et al., 2015; Polnok et al., 2004; Sieval et al., 1998; Thanou et al., 2000).

*3.7. Assessment the calibration curves and solubility of curcumin*

The lambda max (λ max) of curcumin solutions was determined via UV-Vis spectroscopy as 428 nm, and used to measure the maximum solubility of curcumin, and also the encapsulation efficiency of drug loading with nanoparticles from formulations 12 and 26 for $MPC_{100}$-$DPA_{100}$ and $MPC_{30}$-$DPA_{100}$. Linearity was evident from 0 – 12 mg/L curcumin concentration in formulation 12, (ethanol-isopropanol) solvent mix ($R^2$ = 0.9999) and also in formulation 26, (methanol-ethanol-chloroform-acetonitrile) solvent mix ($R^2$ = 0.9997), and from 0 – 10 mg/L for the PBS-methanol (pH 1.6) mix ($R^2$ = 0.9996) where y = 0.1462x + 0.0033. Using the standard curves, the solubility of curcumin in formulation 12 (ethanol-isopropanol), y = 0.1239x + 0.0114, was determined as 3.49 ± 0.14 g/L, and in formulation 26 (methanol-ethanol-chloroform-acetonitrile), y = 0.1315x + 0.0141, as 24.54 ± 1.26 g/L, respectively, indicating solvent associated solubility differences.

*3.8. Curcumin loading and TMC coating*

As described earlier, two contrasting methods, nanoprecipitation and film rehydration, were used to prepare curcumin loaded MPC-DPA nanoparticles. The size and morphology of these nanoparticles were then assessed, together with the drug loading efficiency. The DLS data, as shown in Table 9, for nanoparticles prepared by nanoprecipitation, indicated that mean particle diameters were circa 154 nm and 188 nm when empty, and 142 nm and 175 nm after loading using curcumin saturated solvents, for formulations 26 ($MPC_{30}$-$DPA_{100}$) and 12 ($MPC_{100}$-$DPA_{100}$) respectively. These reductions in mean particle diameter may be the result of the hydrophobic curcumin acting as an increased focus of attraction for the hydrophobic DPA copolymer domains during the hydrophobic effect partitioning of curcumin into the nanoparticles, and hence causing nanoparticle diameter contraction. The addition of TMC (1 mg/mL) to the aqueous nanoprecipitated nanoparticle suspensions resulted in decreased mean particle diameters of circa 136 nm and 162 nm for formulations 26 and 12 respectively, possibly due to filtration (0.22 μm) associated particle exclusion, extrusion, and average size reduction, or the TMC attenuating the previously fully hydrated, and nanoparticle surface extended, MPC copolymer branches. Polydispersity values ranged from 0.08 to 0.18, with formulation 26 ($MPC_{30}$-$DPA_{100}$) displaying the lower values. The film rehydration prepared samples were circa 139 nm and 154 nm when empty, and circa 153 nm and 164 nm when loaded with curcumin, for formulations 26 ($MPC_{30}$-$DPA_{100}$) and 12 ($MPC_{100}$-$DPA_{100}$) respectively, as seen in Table 10. This was the inverse of the effect seen with nanoprecipitation, with the nanoparticles becoming larger in this instance, however given the apparent complexity of film rehydration

nanoparticle morphologies and populations, the greater amount of curcumin loading achieved, and the possibility that curcumin may have resulted in an increased level of copolymer nanoparticle aggregation, this could thus explain the increased diameters observed. In a similar mode to the nanoprecipitation samples, addition of TMC to the aqueous film rehydration prepared nanoparticle suspensions, again resulted in mean dimeter size reductions, to circa 132 nm and 157 nm. Polydispersity values for formulations 26 ($MPC_{30}$-$DPA_{100}$) and 12 ($MPC_{100}$-$DPA_{100}$) ranged from 0.14 to 0.34, with formulation 12 displaying the lower values.

Regarding the surface zeta potential of the unloaded and loaded nanoparticles, Tables 9 and 10, these were initially slightly negative, and close to zero mV when the standard deviation was taken into consideration for unloaded nanoparticles, due to the presence of the amphiphilic groups in MPC polymer structure (Goda et al., 2007), and subsequent curcumin loading shifted the values further to negative. However, following TMC coating of the nanoparticles the zeta potential values shifted and increased to positive values, as the TMC is a polycationic polymer, and as such coated the MPC-DPA nanoparticles due to attractive electrostatic forces between cationic amine groups in TMC polymer and amphiphilic phosphorylcholine groups in MPC (Patrulea et al., 2015; Sahni et al., 2008; Sieval et al., 1998). The shift to positive zeta potential values was more pronounced and consistent with the $MPC_{30}$-$DPA_{100}$ polymer, as the smaller $MPC_{30}$ group was unable to counter the positive charge addition of the TMC, whilst the larger $MPC_{100}$ group polymer was able to more effectively reduce the TMC addition effects on particle surface charge.

The curcumin encapsulation efficiency and loading capacity of the MPC-DPA nanoparticles were low, and indeed undetectable via UV-Vis for $MPC_{30}$-$DPA_{100}$, as seen in Tables 9 and 10, possibly due to the differing amounts of curcumin present in the saturated solutions used, 24.54 g/L and 3.49 g/L curcumin for $MPC_{30}$-$DPA_{100}$ and $MPC_{100}$-$DPA_{100}$, respectively, and resulting from the different levels of curcumin solubility in the solvents used. When the organic solvent phase of formulation 26, containing $MPC_{30}$-$DPA_{100}$, was added to the aqueous PBS phase, it may have precipitated due to formation of a solid dispersion of large micro particles. This would have been the result of the high binding affinity hydrophobic forces between the concentrated curcumin (24.54 g/L) and the DPA copolymer domain (Onoue et al., 2014, 2013; Suzuki et al., 2016). The curcumin nanoparticles would then be lost by filtration (0.22 μm) immediately prior to UV-Vis measurement.

In contrast, the $MPC_{100}$-$DPA_{100}$ copolymer formed curcumin encapsulated nanoparticles, having used a lower concentration of curcumin (3.49 g/L), with UV-Vis detectable and quantifiable levels of curcumin entrapped (Tables 9 and 10). Previous reports have indicated that curcumin inhibits the migration, invasion, proliferation,

and viability of A549, CL1-5, and H1299 human lung cancer cell lines (Pillai et al., 2004; Chen et al., 2008; Lin et al., 2009; Patil et al., 2015). For example, Chen et al., 2008 reported a curcumin concentration dependent effective range of 1 – 20 µM against A549 and CL1-5 cells, and more recently Patil et al., 2015 found that curcumin at 2.9 µg/mL inhibited A549 cell growth. In this current study, the film rehydration prepared $MPC_{100}$-$DPA_{100}$, formulation 12, nanoparticle data shown in Table 10 indicates that curcumin loading of 6.86 µg/mL (18 µM) and 42.57 µg/mL (115 µM) was achieved for MPC-DPA nanoparticles, and TMC coated MPC-DPA nanoparticles respectively. Therefore both of these have sufficient curcumin loading to be considered potentially effective against human lung cancer cells. The nanoprecipitation prepared $MPC_{100}$-$DPA_{100}$, formulation 12, nanoparticle data shown in Table 9 indicates that curcumin loading at 0.92 µg/mL (2.5 µM) and 0.85 µg/mL (2.3 µM) were achieved for MPC-DPA nanoparticles, and TMC coated MPC-DPA nanoparticles respectively, and these levels of curcumin loading are located at the lower end of the effective range (1 – 20 µM) suggested by Chen et al., 2008. However, in this current study the nanoprecipitation was undertaken at a MPC-DPA copolymer in PBS concentration of 0.4 mg/mL, whilst it has been reported previously (Salvage et al., 2016) that $MPC_{100}$-$DPA_{100}$ nanoparticles successfully form in PBS at a copolymer concentration of 2 mg/mL. Therefore it should be possible to increase the copolymer concentration, and thus increase curcumin loading, 5-fold, to circa 4.6 µg/mL (12.5 µM) and 4.25 µg/mL (11.5 µM) for MPC-DPA nanoparticles, and TMC coated MPC-DPA nanoparticles respectively, both of which would be within the range reported by Chen et al., 2008 and Patil et al., 2015, as effective against human lung cancer cells.

The morphological study of the curcumin loaded MPC-DPA nanoparticles, using STEM, confirmed that $MPC_{100}$-$DPA_{100}$ copolymer successfully encapsulated curcumin and formed nanoparticles with an irregular spherical morphology using curcumin at low concentration (3.49 g/L), as seen in Figures 8c and 9c, and were consistent with previous reports of curcumin loaded polymer micelles (Patil et al., 2015). In contrast, the STEM imaging (Figures 8 and 9) of $MPC_{30}$-$DPA_{100}$ copolymer nanoparticles and curcumin, revealed an apparent solid dispersion formation when using curcumin at high concentration (24.54 g/L), for both the nanoprecipitation (Figure 8a) and film rehydration (Figure 9a) preparation methods. Interestingly, the addition of TMC to all formulations produced morphological changes in the nanoparticles, with the appearance of vesicle-like droplet morphologies, as seen in Figures 8b, 8d, 9b and 9d. These were suggestive of the TMC polymer coating the outside of the MPC-DPA nanoparticles, and were morphologically consistent with recent reports of poly(ethylene oxide) based polymersomes (Bartenstein et al., 2016).

One of the key requirements for an effective nanoparticle based drug delivery system is the control of size and drug loading, as these parameters are central to achieving good biodistribution and therapeutic efficacy after administration. Four techniques, filtration, centrifugation, size-exclusion chromatography, and density gradient centrifugation, have been reported as successful for purifying and separating heterogeneous nanoparticle solutions into homogenous fractions (Robertson et al., 2016). Therefore, where necessary, the curcumin loaded MPC-DPA nanoparticles developed in this current study, could be further separated and optimised into distinct sizes and shape fractions in order to facilitate their future development for a range of biomedical applications, including inhalation drug delivery. Additionally, the successful coating of the curcumin loaded MPC-DPA nanoparticles with TMC polymer may provide key advantages such as, improved cell permeation and increased curcumin absorption into human cells (Chen et al., 2016; Guan et al., 2012; Panya et al., 2010; Sahni et al., 2008; Zhang et al., 2013). In summary, $MPC_{100}$-$DPA_{100}$ nanoparticles were formed via nanoprecipitation and film rehydration that were of pulmonary delivery size, contained curcumin at anti-tumour concentrations, and could be coated with TMC to further enhance cellular uptake and delivery.

*3.9. Fourier transform infrared spectroscopy*

The vibrational spectrum of the curcumin was consistent with previous reports (Darandale and Vavia, 2013; Mohan et al., 2012; Zhang et al., 2013) and revealed characteristic main bands, as shown in Figure 10a. A sharp peak at 3508 $cm^{-1}$ indicated the presence of the stretching vibration of the phenolic-OH group, and a sharp peak at 1626 $cm^{-1}$ was attributed to vibration of the carbonyl C=O group. The peak at 1601 $cm^{-1}$ was assigned to the enol C=O stretching, and the peak at 1504 $cm^{-1}$ was the symmetric stretching vibration of an aromatic ring (C=C ring). Moreover, alkane C-H group bending vibration was at 1427 $cm^{-1}$, while aromatic C-O stretching vibration was seen at 1272 $cm^{-1}$. C-O-C stretching vibration and aromatic ring-CH bending vibrations were found at 1024 and 961 $cm^{-1}$, respectively, and between 900 and 650 $cm^{-1}$ a forest of out of plane vibration for CH and $CH_2$ (Darandale and Vavia, 2013; Patil et al., 2015; Pecora et al., 2016).

The structure of $MPC_{30}$-$DPA_{100}$ and $MPC_{100}$-$DPA_{100}$ copolymers were also characterised with FTIR. The main bands in both are presented in Figure 10b, the broad peak at 3500-3000 $cm^{-1}$ may be stretching vibration of nitrogen in primary and secondary amine groups (Gao et al., 2013; Zheng et al., 2013), it may also illustrate the presence of residual moisture, bound or unbound water adsorption, in the copolymer as the carbonyl group in the copolymer structure can strongly interact with water molecules and produce hydrogen bonding (Sammon et al., 1998; Szakonyi and Zelkó, 2012). The peaks at 2963 and 2879 $cm^{-1}$ are the stretching vibration of C-H and -

$CH_2$, respectively (Furuzono et al., 2000; Gao et al., 2013), and the sharp peaks at 1724 and 1479 $cm^{-1}$ the carbonyl C=O and C-H bonds. The stretching vibration of the C-N group and ester band C-O group were observed at 1145 and 1064 $cm^{-1}$ (Faccia and Amalvy, 2013). To confirm the chemical groups in MPC and DPA monomers, the peak of the methane group $(CH_3)_2$- CH- in poly DPA was observed at 2963 $cm^{-1}$ (Faccia and Amalvy, 2013; Furuzono et al., 2000; Gao et al., 2013; Yan and Ishihara, 2008; Zheng et al., 2013), while peaks at 1231, 964 and 786 $cm^{-1}$ were attributed to $–POCH_2$-, -$N+(CH_3)_3$ and C-O-P groups in poly MPC, respectively. The FTIR spectra (Figure 10b) of $MPC_{30}$-$DPA_{100}$ and $MPC_{100}$-$DPA_{100}$ copolymers were principally the same, but the intensity of the peak around (3500-3000) $cm^{-1}$ was stronger for $MPC_{100}$-$DPA_{100}$ than $MPC_{30}$-$DPA_{100,}$ due to hygroscopic nature of MPC which over a broad solution pH range can hydrate with circa 15 water molecules (Chen et al., 2007; Ishihara et al., 1992; Yang et al., 2016; Yaseen et al., 2006).

FTIR spectra of chitosan and TMC are presented in Figure 10c. For chitosan, the broad peak at the range (3500-3000) $cm^{-1}$ corresponded to the combined stretching vibration bands for –OH and $–NH_2$ groups while the peak at 2872 $cm^{-1}$ was the asymmetrical and symmetrical stretching vibration of C-H in the glyosidic ring. Additionally, the bands at 1650 and 1590 $cm^{-1}$ were attributed to $–NHCOCH_3$ group stretching vibration and N-H group bending from chitosan structure, correspondingly. The strong band at 1024 $cm^{-1}$ was consistent with the C-O-C peak (Nazar et al., 2011; Patrulea et al., 2016). Regarding the TMC polymer spectrum in Figure 10c, it was clear that the insertion of trimethyl groups in chitosan structure lead to increased intensities of the main peaks such as the intensity of methyl group C-H in two positions: the stretching bands (3000-2900 $cm^{-1}$) as well as the bending bands at (1500-1470 $cm^{-1}$), and the amide stretching bands (1652 $cm^{-1}$) (de Britto et al., 2012; Hansson et al., 2012; Nazar et al., 2011; Patrulea et al., 2016). The results of FTIR analysis of TMC polymer (Figure 10c) corresponded with NMR analysis where all sets of bonds in the chemical structure were visible as evidence of successful synthesis of TMC from chitosan.

When the FTIR data for all components were observed (Figure 10d) there were no discernible shifts of resonance within the physical mixtures of either curcumin or TMC with the MPC-DPA copolymers. However, there were apparent differences when the FTIR of pure curcumin was compared to that of curcumin mixed with $MPC_{30}$-$DPA_{100}$ or $MPC_{100}$-$DPA_{100}$ copolymers in the organic solvents combinations used to prepare formulations 12 and 26, as shown in Figure 10e. In this instance, there were shifts in the majority of peak positions in all of the mixtures examined. In addition, the sharp peak at 3509 $cm^{-1}$, assigned to phenolic-OH groups in curcumin, disappeared in the both formulation 12 and 26 FTIR spectra. This suggested that there had been an interaction

when mixing curcumin at maximum solubility, 24.30 and 3.44 mg/mL, with $MPC_{30}$-$DPA_{100}$ and $MPC_{100}$-$DPA_{100}$ copolymers at 40 mg/mL in the solvents for formulations 12 and 26 during nanoprecipitation and film rehydration. This interaction was more distinct with $MPC_{30}$-$DPA_{100}$ in formulation 26, due the higher concentration of curcumin (24.30 mg/mL) with the higher ratio of hydrophobic DPA polymer, compared to formulation 12, which contained only 3.44 mg/mL of curcumin for the same ratio of $MPC_{100}$ and $DPA_{100}$ polymers. Furthermore, this interaction may be attributed to intermolecular hydrogen bonding between the phenolic-OH groups in curcumin seen at 3508 $cm^{-1}$ and amine groups as well as carbonyl groups in MPC-DPA copolymer structure at 3500-3000 and 1724 $cm^{-1}$, respectively.

The large amount of curcumin used in formulation 26 may have contributed to formation of a solid dispersion between the $MPC_{30}$-$DPA_{100}$ copolymer and curcumin after evaporation of the organic solvents. This would be due to high affinity binding between curcumin and the DPA monomer, via hydrophobic forces, and the high concentration of curcumin used. The solid dispersion, being insoluble in water, was thus unable to form polymersome morphologies when added to aqueous PBS solution (Gupta and Dixit, 2011; Paradkar et al., 2004). Furthermore, when the FTIR spectra for the same mixture of curcumin and MPC-DPA copolymer were compared, with the different concentrations used for nanoprecipitation and film rehydration, the interaction was more detectable, with peak intensity reduced, in the mixture used for nanoprecipitation. This may be due to the higher concentration of copolymer (40 mg/mL) used in nanoprecipitation process (Figures 10e (iv) and 10e (vi)) compared to the film rehydration (5 mg/mL) method (Figures 10e (v) and 10e (vii). The FTIR data were consistent with the STEM image (Figures 8 and 9), encapsulation efficiency, and drug loading capacity data (Tables 9 and 10) for curcumin loaded nanoparticles, which suggested the formation of solid dispersions of curcumin and $MPC_{30}$-$DPA_{100}$ copolymer, containing large insoluble particles. In summary, $MPC_{100}$-$DPA_{100}$ copolymer displayed a more effective ability to form curcumin encapsulated nanoparticles when using curcumin at low concentration, and therefore the drug quantity used for entrapment has the potential to affect the micellisation and nanoparticle formation processes with MPC-DPA copolymers.

## 4. Conclusions

In conclusion, this current work reported for the first time, by application of a 31 solvent matrix, a novel and comprehensive investigation of solvent choice effects on nanoprecipitation assembled MPC-DPA nanoparticles. The resultant novel data was used to select candidate systems deemed as potentially suitable for inhalation drug

delivery applications, based on particle size and polydispersity, for further assessment and comparison with equivalent film-rehydration MPC-DPA assembled systems. Analysis of this second novel data set afforded further selective testing in the form of curcumin loading and TMC particle coating, leading to the optimisation of MPC-DPA nanoparticle systems with curcumin loading levels reported as effective against human lung cancer cells. The systems prepared and optimised are thus considered suitable for progression to inhalation delivery characterisation, and *in-vitro* human lung cancer cell drug delivery testing. It is believed that this is the first report of curcumin loaded MPC-DPA nanoparticle systems, illustrating their potential to act as a delivery vehicle for the emerging therapeutic compound curcumin. In doing so, this study contributed towards development of novel curcumin nano-formulations with potential pharmaceutical applications for pulmonary delivered treatment of human lung cancer, and is thus of societal interest, benefit, and significance.

**Acknowledgements**

The authors gratefully acknowledge the Council for At-Risk Academics (CARA) and the University of Brighton for supporting this work, Biocompatibles UK Ltd for provision of MPC, and Prof Steven Armes (University of Sheffield, UK) for supplying the test polymers.

**References**

Ahmed, F., Pakunlu, R.I., Brannan, A., Bates, F., Minko, T., Discher, D.E., 2006. Biodegradable polymersomes loaded with both paclitaxel and doxorubicin permeate and shrink tumors, inducing apoptosis in proportion to accumulated drug. J. Control. Release 116, 150–158. doi:10.1016/j.jconrel.2006.07.012

Alexandridis, P., Spontak, R.J., 1999. Solvent-regulated ordering in block copolymers. Curr. Opin. Colloid Interface Sci. 4, 130–139. doi:10.1016/S1359-0294(99)00022-9

Amidi, M., Romeijn, S.G., Borchard, G., Junginger, H.E., Hennink, W.E., Jiskoot, W., 2006. Preparation and characterization of protein-loaded N-trimethyl chitosan nanoparticles as nasal delivery system. J. Control. Release 111, 107–116. doi:10.1016/j.jconrel.2005.11.014

Ayen, W.Y., Garkhal, K., Kumar, N., 2011. Doxorubicin-loaded (PEG)3-PLA nanopolymersomes: Effect of solvents and process parameters on formulation development and in vitro study. Mol. Pharm. 8, 466–478. doi:10.1021/mp1003256

Baka, E., Comer, J.E.A., Takács-Novák, K., 2008. Study of equilibrium solubility measurement by saturation shake-flask method using hydrochlorothiazide as model compound. J. Pharm. Biomed. Anal. 46, 335–341.

doi:10.1016/j.jpba.2007.10.030

Barnett, a H., 2004. Exubera inhaled insulin: a review. Int. J. Clin. Pract. 58, 394–401.

Basnet, P., Skalko-Basnet, N., 2011. Curcumin: An anti-inflammatory molecule from a curry spice on the path to cancer treatment. Molecules 16, 4567–4598. doi:10.3390/molecules16064567

Battaglia, G., LoPresti, C., Massignani, M., Warren, N.J., Madsen, J., Forster, S., Vasilev, C., Hobbs, J.K., Armes, S.P., Chirasatitsin, S., Engler, A.J., 2011. Wet Nanoscale Imaging and Testing of Polymersomes. Small 7, 2010–2015. doi:10.1002/smll.201100511

Battaglia, G., Ryan, A.J., 2006. Pathways of polymeric vesicle formation. J. Phys. Chem. B 110, 10272–10279. doi:10.1021/jp060728n

Bertenstein, J.E., Robertson J., Battaglia, G., Briscoe, W.H., 2016. Colloids and Surfaces A: Physicochemical and Engineering Aspects. 506, 739-746.

Betbeder, D., Lipka, E., Howsam, M., Carpentier, R., 2015. Evolution of availability of curcumin inside poly-lactic-co-glycolic acid nanoparticles : impact on antioxidant and antinitrosant properties. Int. J. Nanomedicine 10, 5355–5366.

Bilati, U., Allémann, E., Doelker, E., 2005. Development of a nanoprecipitation method intended for the entrapment of hydrophilic drugs into nanoparticles. Eur. J. Pharm. Sci. 24, 67–75. doi:10.1016/j.ejps.2004.09.011

Blanazs, A., Armes, S.P., Ryan, A.J., 2009. Self-Assembled Block Copolymer Aggregates: From Micelles to Vesicles and their Biological Applications. Macromol. Rapid Commun. 30, 267–277. doi:10.1002/marc.200800713

Bowen, W.R., Hilal, N., Lovitt, R.W., Wright, C.J., 1998. A new technique for membrane characterisation:direct measurement of the force of adhesion of a single particle using an atomic force microscope. J. Memb. Sci. 139, 269–274.

Canton, I., Massignani, M., Patikarnmonthon, N., Chierico, L., Robertson, J., Renshaw, S. a., Warren, N.J., Madsen, J.P., Armes, S.P., Lewis, A.L., Battaglia, G., 2013. Fully synthetic polymer vesicles for intracellular delivery of antibodies in live cells. FASEB J. 27, 98–108. doi:10.1096/fj.12-212183

Chen, H.W, Lee, J.Y., Huang, J.Y., Wang, C.C., Chen, W.J., Su, S.F., Huang, C.W., Ho, C.C., Chen, J.J.W., Tsai, M.F., Yu, S.L., Yang, P.C., 2008. Curcumin inhibits lung cancer cell invasion and metastasis through tumor suppressor HLJ1. Cancer Research. 68, 7428-7438.

Chen, M., Briscoe, W.H., Armes, S.P., Cohen, H., Klein, J., 2007. Robust, biomimetic polymer brush layers

grown directly from a planar mica surface. ChemPhysChem 8, 1303–1306. doi:10.1002/cphc.200700131

Chen, W., Yuan, Z.-Q., Liu, Y., Zhang, C., Li, J., Zhu, W., Li, F., Zhou, X., Lin, Y., Zhang, X., 2016. Liposomes coated with N -trimethyl chitosan to improve the absorption of harmine in vivo and in vitro. Int. J. Nanomedicine 11, 325–336. doi:10.2147/IJN.S95540

Cipolla, D., Gonda, I., Chan, H.-K., 2013. Liposomal formulations for inhalation. Ther. Deliv. 4, 1047–72. doi:10.4155/tde.13.71

Colley, H.E., Hearnden, V., Avila-Olias, M., Cecchin, D., Canton, I., Madsen, J., Macneil, S., Warren, N., Hu, K., McKeating, J. a., Armes, S.P., Murdoch, C., Thornhill, M.H., Battaglia, G., 2014. Polymersome-mediated delivery of combination anticancer therapy to head and neck cancer cells: 2D and 3D in vitro evaluation. Mol. Pharm. 11, 1176–1188. doi:10.1021/mp400610b

Darandale, S.S., Vavia, P.R., 2013. Cyclodextrin-based nanosponges of curcumin: Formulation and physicochemical characterization. J. Incl. Phenom. Macrocycl. Chem. 75, 315–322. doi:10.1007/s10847-012-0186-9

de Britto, D., de Moura, M.R., Aouada, F.A., Mattoso, L.H.C., Assis, O.B.G., 2012. N,N,N-trimethyl chitosan nanoparticles as a vitamin carrier system. Food Hydrocoll. 27, 487–493. doi:10.1016/j.foodhyd.2011.09.002

Derry, M.J., Fielding, L.A., Armes, S.P., 2016. Polymerization-induced self-assembly of block copolymer nanoparticles via RAFT non-aqueous dispersion polymerization. Prog. Polym. Sci. 52, 1–18. doi:10.1016/j.progpolymsci.2015.10.002

Discher, D.E., Ahmed, F., 2006. Polymersomes. Annu. Rev. Biomed. Eng. 8, 323–341.

Discher, D.E., Ortiz, V., Srinivas, G., Klein, M.L., Kim, Y., Christian, D., Cai, S., Photos, P., Ahmed, F., 2007. Emerging applications of polymersomes in delivery: From molecular dynamics to shrinkage of tumors. Prog. Polym. Sci. 32, 838–857. doi:10.1016/j.progpolymsci.2007.05.011

Du, J., Tang, Y., Lewis, A.L., Armes, S.P., 2005. pH-sensitive vesicles based on a biocompatible zwitterionic diblock copolymer. J. Am. Chem. Soc. 127, 17982–17983. doi:10.1021/ja056514l

Edmondson, S., Nguyen, N.T., Lewis, A.L., Armes, S.P., 2010. Co-Nonsolvency Effects for Surface-Initiated Poly(2-(methacryloyloxy)ethyl phosphorylcholine) Brushes in Alcohol/Water Mixtures. Langmuir 26, 7216–7226. doi:10.1021/la904346j

El-Sherbiny, I.M., El-Baz, N.M., 2015. A Review on Bionanocomposites Based on Chitosan and Its Derivatives for Biomedical Applications, in: Eco-Friendly Polymer Nanocomposites. Springer India, pp. 173–208.

doi:10.1007/978-81-322-2473-0

Faccia, P.A., Amalvy, J.I., 2013. Synthesis, characterization, and swelling behavior of new pH-sensitive hydrogels derived from copolymers of 2-hydroxyethyl methacrylate and 2-(diisopropylamino)ethylmethacrylate. J. Appl. Polym. Sci. 127, 1974–1980. doi:10.1002/app.37576

Furuzono, T., Ishihara, K., Nakabayashi, N., Tamada, Y., 2000. Chemical modi " cation of silk " broin with 2-methacryloyloxyethyl phosphorylcholine . II . Graft-polymerization onto fabric through 2-methacryloyloxyethyl isocyanate and interaction between fabric and platelets 21, 327–333.

Gao, B., Feng, Y., Lu, J., Zhang, L., Zhao, M., Shi, C., Khan, M., Guo, J., 2013. Grafting of phosphorylcholine functional groups on polycarbonate urethane surface for resisting platelet adhesion. Mater. Sci. Eng. C 33, 2871–2878. doi:10.1016/j.msec.2013.03.007

Garbuzenko, O.B., Mainelis, G., Taratula, O., Minko, T., 2014. Inhalation treatment of lung cancer: the influence of composition, size and shape of nanocarriers on their lung accumulation and retention. Cancer Biol. Med. 11, 44–55. doi:http://dx.doi.org/10.7497/j.issn.2095-3941.2014.01.004

Giacomelli, C., Le Men, L., Borsali, R., Lai-Kee-Him, J., Brisson, A., Armes, S.P., Lewis, A.L., 2006. Phosphorylcholine-based pH-responsive diblock copolymer micelles as drug delivery vehicles: Light scattering, electron microscopy and fluorescence experiments. Biomacromolecules 7, 817–828. doi:10.1021/bm0508921

Goda, T., Konno, T., Takai, M., Ishihara, K., 2007. Photoinduced phospholipid polymer grafting on Parylene film: Advanced lubrication and antibiofouling properties. Colloids Surfaces B Biointerfaces 54, 67–73. doi:10.1016/j.colsurfb.2006.09.006

Gou, M., Men, K., Shi, H., Xiang, M., Zhang, J., Song, J., Long, J., Wan, Y., Luo, F., Zhao, X., Qian, Z., 2011. Curcumin-loaded biodegradable polymeric micelles for colon cancer therapy in vitro and in vivo. Nanoscale 3, 1558–67. doi:10.1039/c0nr00758g

Gratton, S.E. a, Ropp, P. a, Pohlhaus, P.D., Luft, J.C., Madden, V.J., Napier, M.E., DeSimone, J.M., 2008. The effect of particle design on cellular internalization pathways. Proc. Natl. Acad. Sci. U. S. A. 105, 11613–11618. doi:10.1073/pnas.0801763105

Guan, M., Zhou, Y., Zhu, Q.L., Liu, Y., Bei, Y.Y., Zhang, X.N., Zhang, Q., 2012. N-trimethyl chitosan nanoparticle-encapsulated lactosyl-norcantharidin for liver cancer therapy with high targeting efficacy. Nanomedicine Nanotechnology, Biol. Med. 8, 1172–1181. doi:10.1016/j.nano.2012.01.009

Gupta, N.K., Dixit, V.K., 2011. Bioavailability enhancement of curcumin by complexation with phosphatidyl

choline. J. Pharm. Sci. 100, 1987–1995. doi:10.1002/jps.22393

Hansson, A., Hashom, N., Falson, F., Rousselle, P., Jordan, O., Borchard, G., 2012. In vitro evaluation of an RGD-functionalized chitosan derivative for enhanced cell adhesion. Carbohydr. Polym. 90, 1494–1500. doi:10.1016/j.carbpol.2012.07.020

Hu, X., Yang, F.-F., Quan, L.-H., Liu, C.-Y., Liu, X.-M., Ehrhardt, C., Liao, Y.-H., 2014. Pulmonary delivered polymeric micelles--pharmacokinetic evaluation and biodistribution studies. Eur. J. Pharm. Biopharm. 88, 1064–75. doi:10.1016/j.ejpb.2014.10.010

Ishihara, K., Oshida, H., Endo, Y., Ueda, T., Watanabe, A., Nakabayashi, N., 1992. Hemocompatibility of human whole blood on polymers with a phospholipid polar group and its mechanism. J. Biomed. Mater. Res. 26, 1543–1552. doi:10.1002/jbm.820261202

Israelachvili, J.N., 2011. Intermolecular and surface forces, in: Academic Press, USA. doi:10.1002/elps.201000212

Kakran, M., Sahoo, N.G., Tan, I.L., Li, L., 2012. Preparation of nanoparticles of poorly water-soluble antioxidant curcumin by antisolvent precipitation methods. J. Nanoparticle Res. 14. doi:10.1007/s11051-012-0757-0

Koshkina, N. V, Waldrep, J.C., Roberts, L.E., Golunski, E., Melton, S., 2001. Paclitaxel liposome aerosol treatment induces inhibition of pulmonary metastases in murine renal carcinoma model 1. Clin Cancer Res. 7, 3258–3262.

Kuzmov, A., Minko, T., 2015. Nanotechnology approaches for inhalation treatment of lung diseases. J. Control. Release 219, 500–518. doi:10.1016/j.jconrel.2015.07.024

Lavertu, M., Xia, Z., Serreqi, A.N., Berrada, M., Rodrigues, A., Wang, D., Buschmann, M.D., Gupta, A., 2003. A validated 1H NMR method for the determination of the degree of deacetylation of chitosan. J. Pharm. Biomed. Anal. 32, 1149–1158. doi:10.1016/S0731-7085(03)00155-9

Licciardi, M., Craparo, E.F., Giammona, G., Armes, S.P., Tang, Y., Lewis, A.L., 2008. in Vitro Biological Evaluation of Folate-Functionalized Block Copolymer Micelles for Selective Anti-Cancer Drug Delivery. Macromol. Biosci. 8, 615–26. doi:10.1002/mabi.200800009

Licciardi, M., Giammona, G., Du, J.Z., Armes, S.P., Tang, Y.Q., Lewis, A.L., 2006. New folate-functionalized biocompatible block copolymer micelles as potential anti-cancer drug delivery systems. Polymer (Guildf). 47, 2946–2955.

Licciardi, M., Tang, Y., Billingham, N.C., Armes, S.P., 2005. Synthesis of novel folate-functionalized

biocompatible block copolymers by atom transfer radical polymerization for gene delivery and encapsulation of hydrophobic drugs. Biomacromolecules 6, 1085–1096.

Lin S.S., Lai, K.C., Hsu, S.C., Yang, J.S., Kuo, C.L., Lin, J.P., Ma, Y.S., Wu, C.C., Chung, J.G., 2009. Curcumin inhibits the migration and invasion of human A549 lung cancer cells through the inhibition matrix metalloproteinase-2 and -9 and vascular endothelial growth factor (VEGF). Cancer Letters. 285, 127-133.

Liu, K.N., Lai, C.M., Lee, Y.T., Wang, S.N., Chen, R.P.Y., Jan, J.S., Liu, H.S., Wang, S.S.S., 2012. Curcumin's pre-incubation temperature affects its inhibitory potency toward amyloid fibrillation and fibril-induced cytotoxicity of lysozyme. Biochim. Biophys. Acta - Gen. Subj. 1820, 1774–1786. doi:10.1016/j.bbagen.2012.07.012

Lomas, H., Canton, I., MacNeil, S., Du, J., Armes, S.P., Ryan, A.J., Lewis, A.L., Battaglia, G., 2007. Biomimetic pH sensitive polymersomes for efficient DNA encapsulation and delivery. Adv. Mater. 19, 4238–4243. doi:10.1002/adma.200700941

Lomas, H., Du, J., Canton, I., Madsen, J., Warren, N., Armes, S.P., Lewis, A.L., Battaglia, G., 2010. Efficient encapsulation of plasmid DNA in pH-sensitive PMPC-PDPA polymersomes: study of the effect of PDPA block length on copolymer-DNA binding affinity. Macromol. Biosci. 10, 513–530. doi:10.1002/mabi.201000083

Lomas, H., Massignani, M., Abdullah, K. a, Canton, I., Lo Presti, C., MacNeil, S., Du, J., Blanazs, A., Madsen, J., Armes, S.P., Lewis, A.L., Battaglia, G., 2008. Non-cytotoxic polymer vesicles for rapid and efficient intracellular delivery. Faraday Discuss. 139, 143–159. doi:10.1039/b717431d

Ma, Y., Tang, Y., Billingham, N.C., Armes, S.P., Lewis, A.L., Lloyd, A.W., Salvage, J.P., 2003. Well-defined biocompatible block copolymers via atom transfer radical polymerization of 2-methacryloyloxyethyl phosphorylcholine in protic media. Macromolecules 36, 3475–3484. doi:10.1021/ma021762c

Mack, G.S., 2007. Pfizer dumps Exubera. Nat. Biotechnol. 25, 1331–1332. doi:10.1038/nbt1207-1331

Messager, L., Gaitzsch, J., Chierico, L., Battaglia, G., 2014. Novel aspects of encapsulation and delivery using polymersomes. Curr Opin Pharmacol 18, 104–111. doi:10.1016/j.coph.2014.09.017

Meyer, E.E., Rosenberg, K.J., Israelachvili, J., 2006. Recent progress in understanding hydrophobic interactions. Proc. Natl. Acad. Sci. U.S.A. 103, 15739.

Minko, T., Rodriguez-Rodriguez, L., Pozharov, V., 2013. Nanotechnology approaches for personalized treatment of multidrug resistant cancers. Adv. Drug Deliv. Rev. 65, 1880–1895.

doi:10.1016/j.addr.2013.09.017

Mock, C.D., Jordan, B.C., Selvam, C., 2015. Recent advances of curcumin and its analogues in breast cancer prevention and treatment. RSC Adv. 5, 75575–75588. doi:10.1039/C5RA14925H

Mohan, P.R.K., Sreelakshmi, G., Muraleedharan, C. V., Joseph, R., 2012. Water soluble complexes of curcumin with cyclodextrins: Characterization by FT-Raman spectroscopy. Vib. Spectrosc. 62, 77–84. doi:10.1016/j.vibspec.2012.05.002

Motornov, M., Roiter, Y., Tokarev, I., Minko, S., 2010. Stimuli-responsive nanoparticles, nanogels and capsules for integrated multifunctional intelligent systems. Prog. Polym. Sci. 35, 174–211. doi:10.1016/j.progpolymsci.2009.10.004

Mu, Q.S., Zhao, X.B., Lu, J.R., Armes, S.P., Lewis, a L., Thomas, R.K., 2008. pH-responsive nanoaggregation of diblock phosphorylcholine copolymers. J. Phys. Chem. B 112, 9652–9. doi:10.1021/jp710365u

Nahar, P.P., Slitt, A.L., Seeram, N.P., 2015. Anti-inflammatory effects of novel standardized solid lipid curcumin formulations. J. Med. Food 18, 786–792. doi:10.1089/jmf.2014.0053

Nazar, H., Fatouros, D.G., Van Der Merwe, S.M., Bouropoulos, N., Avgouropoulos, G., Tsibouklis, J., Roldo, M., 2011. Thermosensitive hydrogels for nasal drug delivery: The formulation and characterisation of systems based on N-trimethyl chitosan chloride. Eur. J. Pharm. Biopharm. 77, 225–232. doi:10.1016/j.ejpb.2010.11.022

Onoue, S., Kojo, Y., Suzuki, H., Yuminoki, K., Kou, K., Kawabata, Y., Yamauchi, Y., Hashimoto, N., Yamada, S., 2013. Development of novel solid dispersion of tranilast using amphiphilic block copolymer for improved oral bioavailability. Int. J. Pharm. 452, 220–226. doi:10.1016/j.ijpharm.2013.05.022

Onoue, S., Suzuki, H., Kojo, Y., Matsunaga, S., Sato, H., Mizumoto, T., Yuminoki, K., Hashimoto, N., Yamada, S., 2014. Self-micellizing solid dispersion of cyclosporine A with improved dissolution and oral bioavailability. Eur. J. Pharm. Sci. 62, 16–22. doi:10.1016/j.ejps.2014.05.006

Pillai, G.R., Srivastava, A.S., Hassanein, T.I., Chauhan, D.P., Carrier, E., 2004. Induction of apoptosis in human lung cnacer cells by curcumin. Cancer Letters. 208, 163-170.

Panya, A., Laguerre, M., Lecomte, J., Villeneuve, P., Weiss, J., McClements, D.J., Decker, E.A., 2010. Effects of chitosan and rosmarinate esters on the physical and oxidative stability of liposomes. J. Agric. Food Chem. 58, 5679–5684. doi:10.1021/jf100133b

Paradkar, A., Ambike, A.A., Jadhav, B.K., Mahadik, K.R., 2004. Characterization of curcumin-PVP solid dispersion obtained by spray drying. Int. J. Pharm. 271, 281–286. doi:10.1016/j.ijpharm.2003.11.014

Patikarnmonthon, N., 2013. PMPC-PDPA polymersomes-mediated siRNA delivery. University of Sheffield. doi:10.1007/978-1-4939-3112-5

Patil, S., Choudhary, B., Rathore, A., Roy, K., Mahadik, K., 2015. Enhanced oral bioavailability and anticancer activity of novel curcumin loaded mixed micelles in human lung cancer cells. Phytomedicine 22, 1103–1111. doi:10.1016/j.phymed.2015.08.006

Patrulea, V., Applegate, L.A., Ostafe, V., Jordan, O., Borchard, G., 2015. Optimized synthesis of O-carboxymethyl-N,N,N-trimethyl chitosan. Carbohydr. Polym. 122, 46–52. doi:10.1016/j.carbpol.2014.12.014

Patrulea, V., Hirt-Burri, N., Jeannerat, A., Applegate, L.A., Ostafe, V., Jordan, O., Borchard, G., 2016. Peptide-decorated chitosan derivatives enhance fibroblast adhesion and proliferation in wound healing. Carbohydr. Polym. 142, 114–123. doi:10.1016/j.carbpol.2016.01.045

Pearson, R.T., Warren, N.J., Lewis, A.L., Armes, S.P., 2013. Effect of pH and temperature on PMPC − PDPA copolymer self- assembly. Macromolecules 46, 1400–1407.

Pecora, T.M.G., Cianciolo, S., Catalfo, A., De Guidi, G., Ruozi, B., Cristiano, M.C., Paolino, D., Graziano, A.C.E., Fresta, M., Pignatello, R., 2016. Preparation, characterization and photostability assessment of curcumin microencapsulated within methacrylic copolymers. J. Drug Deliv. Sci. Technol. 33, 88–97. doi:10.1016/j.jddst.2016.03.013

Pegoraro, C., Cecchin, D., Gracia, L.S., Warren, N., Madsen, J., Armes, S.P., Lewis, A., Macneil, S., Battaglia, G., 2013. Enhanced drug delivery to melanoma cells using PMPC-PDPA polymersomes. Cancer Lett. 334, 328–37. doi:10.1016/j.canlet.2013.02.007

Pegoraro, C., Cecchin, D., Madsen, J., Warren, N., Armes, S.P., MacNeil, S., Lewis, A., Battaglia, G., 2014. Translocation of flexible polymersomes across pores at the nanoscale. Biomater. Sci. 2, 680. doi:10.1039/c3bm60294j

Polnok, A., Borchard, G., Verhoef, J.C., Sarisuta, N., Junginger, H.E., 2004. Influence of methylation process on the degree of quaternization of N-trimethyl chitosan chloride. Eur. J. Pharm. Biopharm. 57, 77–83. doi:10.1016/S0939-6411(03)00151-6

Porto, L.C., Aissou, K., Giacomelli, C., Baron, T., Rochas, C., Pignot-Paintrand, I., Armes, S.P., Lewis, A.L., Soldi, V., Borsali, R., 2011. Nanostructured films made from zwitterionic phosphorylcholine diblock copolymer systems. Macromolecules 44, 2240–2244. doi:10.1021/ma1029554

Prasad, S., Gupta, S.C., Tyagi, A.K., Aggarwal, B.B., 2014. Curcumin, a component of golden spice: From

bedside to bench and back. Biotechnol. Adv. 32, 1053–1064. doi:10.1016/j.biotechadv.2014.04.004

Robertson, J.D., Rizzello, L., Avila-Olias, M., Gaitzsch, J., Contini, C., Magoń, M.S., Renshaw, S.A., Battaglia, G., 2016. Purification of Nanoparticles by Size and Shape. Sci. Rep. 6, 27494. doi:10.1038/srep27494

Robertson, J.D., Yealland, G., Avila-Olias, M., Chierico, L., Bandmann, O., Renshaw, S. a, Battaglia, G., 2014. pH-sensitive tubular polymersomes: formation and applications in cellular delivery. ACS Nano 8, 4650–61. doi:10.1021/nn5004088

Sadeghi, F., Ashofteh, M., Homayouni, A., Abbaspour, M., Nokhodchi, A., Garekani, H.A., 2016. Antisolvent precipitation technique: A very promising approach to crystallize curcumin in presence of polyvinyl pyrrolidon for solubility and dissolution enhancement. Colloids Surfaces B Biointerfaces 147, 258–264. doi:10.1016/j.colsurfb.2016.08.004

Saengkrit, N., Saesoo, S., Srinuanchai, W., Phunpee, S., Ruktanonchai, U.R., 2014. Influence of curcumin-loaded cationic liposome on anticancer activity for cervical cancer therapy. Colloids Surfaces B Biointerfaces 114, 349–356. doi:10.1016/j.colsurfb.2013.10.005

Sahni, J.K., Chopra, S., Ahmad, F.J., Khar, R.K., 2008. Potential prospects of chitosan derivative trimethyl chitosan chloride (TMC) as a polymeric absorption enhancer: synthesis, characterization and applications. J. Pharm. Pharmacol. 60, 1111–9. doi:10.1211/jpp.60.9.0001

Salvage, J.P., Rose, S.F., Phillips, G.J., Hanlon, G.W., Lloyd, A.W., Ma, I.Y., Armes, S.P., Billingham, N.C., Lewis, A.L., 2005. Novel biocompatible phosphorylcholine-based self-assembled nanoparticles for drug delivery. J. Control. Release 104, 259–70. doi:10.1016/j.jconrel.2005.02.003

Salvage, J.P., Smith, T., Lu, T., Sanghera, A., Standen, G., Tang, Y., Lewis, A.L., 2016. Synthesis, characterisation, and in vitro cellular uptake kinetics of nanoprecipitated poly(2-methacryloyloxyethyl phosphorylcholine)-b-poly(2-(diisopropylamino)ethyl methacrylate) (MPC-DPA) polymeric nanoparticle micelles for nanomedicine applications. Appl. Nanosci. 1–22. doi:10.1007/s13204-016-0520-4

Salvage, J.P., Thom, C., Lewis, A.L., Phillips, G.J., Lloyd, A.W., 2015. Nanoprecipitation of polymeric nanoparticle micelles based on 2-methacryloyloxyethyl phosphorylcholine (MPC) with 2-(diisopropylamino)ethyl methacrylate (DPA), for intracellular delivery applications. J. Mater. Sci. Mater. Med. 26, 150. doi:10.1007/s10856-015-5480-9

Sammon, C., Mura, C., Yarwood, J., Everall, N., Swart, R., Hodge, D., Hallam, S., Uni, V., Campus, C., Sheffield, S., 1998. FTIR - ATR studies of the structure and dynamics of water molecules in polymeric matrixes . A comparison of PET and PVC. J. Phys. Chem. B 102, 3402–3411.

Schubert, M.A., Muller-Goymann, C.C., 2003. Solvent injection as a new approach for manufacturing lipid nanoparticles - Evaluation of the method and process parameters. Eur. J. Pharm. Biopharm. 55, 125–131.

Shanmugam, M.K., Rane, G., Kanchi, M.M., Arfuso, F., Chinnathambi, A., Zayed, M.E., Alharbi, S.A., Tan, B.K.H., Kumar, A.P., Sethi, G., 2015. The multifaceted role of curcumin in cancer prevention and treatment, Molecules. doi:10.3390/molecules20022728

Sieval, A., Thanoua, M., Kotze, A., Verhoef, J., Brussee, J., Junginger, H., 1998. Preparation and NMR characterization of highly substitited N-trimethyl chitosan chloride. Carbohydr. Polym. 36, 157–165.

Smallwood, I.M., 1996. Handbook of Organic Solvent Properties, First. ed, Arnold, London. doi:10.1016/B978-0-08-052378-1.50026-8

Sorrell, I., Shipley, R.J., Hearnden, V., Colley, H.E., Thornhill, M.H., Murdoch, C., Webb, S.D., 2014. Combined mathematical modelling and experimentation to predict polymersome uptake by oral cancer cells. Nanomedicine 10, 339–48. doi:10.1016/j.nano.2013.08.013

Steed, E., Balda, M.S., Matter, K., 2010. Dynamics and functions of tight junctions. Trends Cell Biol. 20, 142–149. doi:10.1016/j.tcb.2009.12.002

Suzuki, H., Kojo, Y., Yakushiji, K., Yuminoki, K., Hashimoto, N., Onoue, S., 2016. Strategic application of self-micellizing solid dispersion technology to respirable powder formulation of tranilast for improved therapeutic potential. Int. J. Pharm. 499, 255–262. doi:10.1016/j.ijpharm.2015.12.065

Szakonyi, G., Zelkó, R., 2012. The effect of water on the solid state characteristics of pharmaceutical excipients : Molecular mechanisms , measurement techniques , and quality aspects of final dosage form The effect of water on the solid state characteristics of pharmaceutical excipie. doi:10.4103/2230-973X.96922

Thanou, M., Verhoef, J.C., Marbach, P., Junginger, H.E., 2000. Intestinal absorption of octreotide: N-trimethyl chitosan chloride (TMC) ameliorates the permeability and absorption properties of the somatostatin analogue in vitro and in vivo. J. Pharm. Sci. 89, 951–957. doi:10.1002/1520-6017(200007)89:7<951::AID-JPS13>3.0.CO;2-1

Thanou, M.M., Kotzé, A.F., Scharringhausen, T., Lueßen, H.L., De Boer, A.G., Verhoef, J.C., Junginger, H.E., 2000. Effect of degree of quaternization of N-trimethyl chitosan chloride for enhanced transport of hydrophilic compounds across intestinal Caco-2 cell monolayers. J. Control. Release 64, 15–25. doi:10.1016/S0168-3659(99)00131-5

Tomren, M.A., Másson, M., Loftsson, T., Tønnesen, H.H., 2007. Studies on curcumin and curcuminoids. Int. J. Pharm. 338, 27–34. doi:10.1016/j.ijpharm.2007.01.013

Ungaro, F., d'Angelo, I., Miro, A., La Rotonda, M.I., Quaglia, F., 2012. Engineered PLGA nano- and micro-carriers for pulmonary delivery: challenges and promises. J. Pharm. Pharmacol. 64, 1217–1235. doi:10.1111/j.2042-7158.2012.01486.x

Wang, J., Wang, H., Zhu, R., Liu, Q., Fei, J., Wang, S., 2015. Anti-inflammatory activity of curcumin-loaded solid lipid nanoparticles in IL-1?? transgenic mice subjected to the lipopolysaccharide-induced sepsis. Biomaterials 53, 475–483. doi:10.1016/j.biomaterials.2015.02.116

Wang, Y.J., Pan, M.H., Cheng, A.L., Lin, L.I., Ho, Y.S., Hsieh, C.Y., Lin, J.K., 1997. Stability of curcumin in buffer solutions and characterization of its degradation products. J. Pharm. Biomed. Anal. 15, 1867–1876. doi:10.1016/S0731-7085(96)02024-9

Xie, X., Tao, Q., Zou, Y., Zhang, F., Guo, M., Wang, Y., Wang, H., Zhou, Q., Yu, S., 2011. PLGA nanoparticles improve the oral bioavailability of curcumin in rats: Characterizations and mechanisms. J. Agric. Food Chem. 59, 9280–9289. doi:10.1021/jf202135j

Yallapu, M.M., Jaggi, M., Chauhan, S.C., 2010. Scope of nanotechnology in ovarian cancer therapeutics. J. Ovarian Res. 3, 19. doi:10.1186/1757-2215-3-19

Yan, L., Ishihara, K., 2008. Graft copolymerization of 2-methacryloyloxyethyl phosphorylcholine to cellulose in homogeneous media using atom transfer radical polymerization for providing new hemocompatible coating materials. J. Polym. Sci. Part A Polym. Chem. doi:10.1002/pola

Yang, T., Choi, S.K., Lee, Y.R., Cho, Y., Kim, J.W., 2016. Novel associative nanoparticles grafted with hydrophobically modified zwitterionic polymer brushes for the rheological control of aqueous polymer gel fluids. Polym. Chem. doi:10.1039/C6PY00359A

Yaseen, M., Lu, J.R., Webster, J.R.P., Penfold, J., 2006. The structure of zwitterionic phosphocholine surfactant monolayers. Langmuir 22, 5825–5832. doi:10.1021/la053316z

Ye, X., Niroomand, H., Hu, S., Khomami, B., 2015. Block copolymer micelle formation in a solvent good for all the blocks. Colloid Polym. Sci. 293, 2799–2805. doi:10.1007/s00396-015-3658-9

Yealland, G., 2015. Polymersome Mediated Delivery of Mitochondrial Therapeutics to parkin Mutant Fibroblasts by. PhD Thesis, Univ. Sheff.

Yoshikawa, H.Y., Rossetti, F.F., Kaufmann, S., Kaindl, T., Madsen, J., Engel, U., Lewis, A.L., Armes, S.P., Tanaka, M., 2011. Quantitative evaluation of mechanosensing of cells on dynamically tunable hydrogels. J. Am. Chem. Soc. 133, 1367–1374. doi:10.1021/ja1060615

Zhang, J., Tang, Q., Xu, X., Li, N., 2013. Development and evaluation of a novel phytosome-loaded chitosan

microsphere system for curcumin delivery. Int. J. Pharm. 448, 168–174. doi:10.1016/j.ijpharm.2013.03.021

Zheng, Z., Ren, L., Zhai, Z., Wang, Y., Hang, F., 2013. Surface modification on polyethylene terephthalate fi lms with 2-methacryloyloxyethyl phosphorylcholine. Mater. Sci. Eng. C 33, 3041–3046. doi:10.1016/j.msec.2013.03.036

**Tables**

**Table 1**
Classification of organic solvent properties (adapted from (Smallwood, 1996)).

| Solvent Name | Polarity Value | Solubility in Water (25°C, % w/w) | Absolute Viscosity (25 °C, Cp) | Boiling Point (°C) |
|---|---|---|---|---|
| **Methanol** | 76.2 | Total | 0.6 | 64 |
| **Ethanol** | 65.4 | Total | 1.08 | 78 |
| **Isopropanol** | 54.6 | Total | 2.0 | 82 |
| **Acetonitrile** | 46.0 | Total | 0.38 | 81.6 |
| **Chloroform** | 25.9 | 0.82 | 0.57 | 61 |

**Table 2**
The 31 solvent combination matrix used to assess MPC-DPA copolymer solubility at 40 mg/mL

| | Solvent combination ratios | | | | | |
|---|---|---|---|---|---|---|
| # | Methanol | Ethanol | Chloroform | Acetonitrile | Isopropanol | Ratio |
| 1 | 1 | 0 | 0 | 0 | 0 | 1:0:0:0:0 |
| 2 | 0 | 1 | 0 | 0 | 0 | 0:1:0:0:0 |
| 3 | 0 | 0 | 1 | 0 | 0 | 0:0:1:0:0 |
| 4 | 0 | 0 | 0 | 1 | 0 | 0:0:0:1:0 |
| 5 | 0 | 0 | 0 | 0 | 1 | 0:0:0:0:1 |
| 6 | 1 | 1 | 0 | 0 | 0 | 1:1:0:0:0 |
| 7 | 1 | 0 | 1 | 0 | 0 | 1:0:1:0:0 |
| 8 | 1 | 0 | 0 | 1 | 0 | 1:0:0:1:0 |
| 9 | 1 | 0 | 0 | 0 | 1 | 1:0:0:0:1 |
| 10 | 0 | 1 | 1 | 0 | 0 | 0:1:1:0:0 |
| 11 | 0 | 1 | 0 | 1 | 0 | 0:1:0:1:0 |
| 12 | 0 | 1 | 0 | 0 | 1 | 0:1:0:0:1 |
| 13 | 0 | 0 | 1 | 1 | 0 | 0:0:1:1:0 |
| 14 | 0 | 0 | 1 | 0 | 1 | 0:0:1:0:1 |
| 15 | 0 | 0 | 0 | 1 | 1 | 0:0:0:1:1 |
| 16 | 1 | 1 | 1 | 0 | 0 | 1:1:1:0:0 |
| 17 | 1 | 1 | 0 | 1 | 0 | 1:1:0:1:0 |
| 18 | 1 | 1 | 0 | 0 | 1 | 1:1:0:0:1 |
| 19 | 0 | 1 | 1 | 1 | 0 | 0:1:1:1:0 |
| 20 | 1 | 0 | 1 | 1 | 0 | 1:0:1:1:0 |
| 21 | 1 | 0 | 1 | 0 | 1 | 1:0:1:0:1 |
| 22 | 1 | 0 | 0 | 1 | 1 | 1:0:0:1:1 |
| 23 | 0 | 1 | 1 | 0 | 1 | 0:1:1:0:1 |
| 24 | 0 | 1 | 0 | 1 | 1 | 0:1:0:1:1 |
| 25 | 0 | 0 | 1 | 1 | 1 | 0:0:1:1:1 |
| 26 | 1 | 1 | 1 | 1 | 0 | 1:1:1:1:0 |
| 27 | 0 | 1 | 1 | 1 | 1 | 0:1:1:1:1 |
| 28 | 1 | 0 | 1 | 1 | 1 | 1:0:1:1:1 |
| 29 | 1 | 1 | 0 | 1 | 1 | 1:1:0:1:1 |
| 30 | 1 | 1 | 1 | 0 | 1 | 1:1:1:0:1 |
| 31 | 1 | 1 | 1 | 1 | 1 | 1:1:1:1:1 |

**Table 3** Molecular weight (Mn and Mw) and polydispersity (Mw/Mn) of MPC-DPA diblock copolymers determined *via* $^{1}$H NMR and organic GPC

| **$MPC_{30}$-$DPA_{100}$** | **Mn** | **Mw** | **Mw/Mn** |
|---|---|---|---|
| Target (g/mol) | 30190 | - | - |
| $^{1}$H NMR | 30190 | - | - |
| GPC | 33050 | 33890 | 1.03 |
| **$MPC_{100}$-$DPA_{100}$** | **Mn** | **Mw** | **Mw/Mn** |
| Target (g/mol) | 50860 | - | - |
| $^{1}$H NMR | 50860 | - | - |
| GPC | 50060 | 50500 | 1.01 |

**Table 4**
Visual classification of MPC-DPA copolymer solubility in solvents. See Table 2 for solvent formulation details.

| Solubility visual classification of MPC-DPA copolymers | | | |
|---|---|---|---|
| # | Solvent Combination | **$MPC_{100}$ – $DPA_{100}$** | **$MPC_{30}$ – $DPA_{100}$** |
| 1 | 1:0:0:0:0 | Completely soluble | Slightly soluble |
| 2 | 0:1:0:0:0 | Completely soluble | Slightly soluble |
| 3 | 0:0:1:0:0 | Practically insoluble | Practically insoluble |
| 4 | 0:0:0:1:0 | Practically insoluble | Practically insoluble |
| 5 | 0:0:0:0:1 | Completely soluble | Completely soluble |
| 6 | 1:1:0:0:0 | Completely soluble | Slightly soluble |
| 7 | 1:0:1:0:0 | Completely soluble | Completely soluble |
| 8 | 1:0:0:1:0 | Completely soluble | Slightly soluble |
| 9 | 1:0:0:0:1 | Completely soluble | Slightly soluble |
| 10 | 0:1:1:0:0 | Completely soluble | Completely soluble |
| 11 | 0:1:0:1:0 | Completely soluble | Slightly soluble |
| 12 | 0:1:0:0:1 | Completely soluble | Completely soluble |
| 13 | 0:0:1:1:0 | Practically insoluble | Practically insoluble |
| 14 | 0:0:1:0:1 | Completely soluble | Completely soluble |
| 15 | 0:0:0:1:1 | Completely soluble | Slightly soluble |
| 16 | 1:1:1:0:0 | Completely soluble | Completely soluble |
| 17 | 1:1:0:1:0 | Completely soluble | Completely soluble |
| 18 | 1:1:0:0:1 | Completely soluble | Slightly soluble |
| 19 | 0:1:1:1:0 | Completely soluble | Completely soluble |
| 20 | 1:0:1:1:0 | Completely soluble | Slightly soluble |
| 21 | 1:0:1:0:1 | Completely soluble | Completely soluble |
| 22 | 1:0:0:1:1 | Completely soluble | Slightly soluble |
| 23 | 0:1:1:0:1 | Completely soluble | Completely soluble |
| 24 | 0:1:0:1:1 | Completely soluble | Completely soluble |
| 25 | 0:0:1:1:1 | Completely soluble | Completely soluble |
| 26 | 1:1:1:1:0 | Completely soluble | Completely soluble |
| 27 | 0:1:1:1:1 | Completely soluble | Completely soluble |
| 28 | 1:0:1:1:1 | Completely soluble | Completely soluble |
| 29 | 1:1:0:1:1 | Completely soluble | Slightly soluble |
| 30 | 1:1:1:0:1 | Completely soluble | Completely soluble |
| 31 | 1:1:1:1:1 | Completely soluble | Completely soluble |

**Table 5**

Solvent effect on size and polydispersity of $MPC_{30}$-$DPA_{100}$ nanoparticle systems prepared via nanoprecipitation (Mean ± SD, n = 3). See Table 2 for solvent formulation details.

| Solvent Combination | | Filter (µm) | Diameter (*ZAve*) (nm) (±SD) | Polydispersity (Pd) (±SD) | *Dh*[1] (nm) (±SD) | *Dh*[2] (nm) (±SD) | *Dh*[3] (nm) (±SD) |
|---|---|---|---|---|---|---|---|
| 1 | 1:0:0:0:0 | - | 57.1 (0.2) | 0.05 (0.02) | 61.1 (0.8) | - | - |
| | | 0.45 | 56.7 (0.3) | 0.04 (0.01) | 60.4 (0.8) | - | - |
| | | 0.22 | 56.5 (0.1) | 0.05 (0.00) | 60.5 (0.4) | - | - |
| 2 | 0:1:0:0:0 | - | 483.6 (8.4) | 0.71 (0.06) | 331.6 (115.3) | 2180.3 (2588.4) | 3459 (2480.9) |
| | | 0.45 | 135.2 (1.9) | 0.15 (0.01) | 160.1 (3.2) | - | - |
| | | 0.22 | 133.6 (2.9) | 0.10 (0.00) | 150.1 (5.0) | - | - |
| 3 | 0:0:1:0:0 | - | - | - | - | - | - |
| 4 | 0:0:0:1:0 | - | - | - | - | - | - |
| 5 | 0:0:0:0:1 | - | 1099.0 (351.5) | 0.93 (0.09) | 233.2 (69.9) | 1994.9 (3088.3) | - |
| | | 0.45 | 167.6 (0.6) | 0.14 (0.02) | 193.0 (9.2) | 1747.7 (3027.0) | - |
| | | 0.22 | 150.2 (7.3) | 0.12 (0.03) | 169.3 (7.9) | 1675 (2901.2) | - |
| 6 | 1:1:0:0:0 | - | 177.6 (28.0) | 0.51 (0.01) | 46.9 (0.5) | 346.1 (28.4) | 1682.7 (2914.5) |
| | | 0.45 | 85.3 (8.7) | 0.43 (0.03) | 141.3 (154.8) | 195.0 (110.9) | 1657 (2870.0) |
| | | 0.22 | 50.6 (4.9) | 0.13 (0.07) | 55.2 (4.7) | 418.7 (725.2) | 1286.3 (2228) |
| 7 | 1:0:1:0:0 | - | 415.4 (176.8) | 0.68 (0.10) | 218.7 (9.4) | 1939.1 (2640.2) | 2047.4 (3052.1) |
| | | 0.45 | 110.1 (95.6) | 0.20 (0.14) | 100.2 (87.3) | 1791.3 (3102.7) | - |
| | | 0.22 | 102.3 (20.8) | 0.41 (0.14) | 9.9 (6.5) | 128.2 (9.1) | 3486.3 (3009.1) |
| 8 | 1:0:0:1:0 | - | 55.7 (0.1) | 0.05 (0.01) | 59.5 (0.5) | - | - |
| | | 0.45 | 55.3 (0.3) | 0.04 (0.00) | 58.8 (0.7) | - | - |
| | | 0.22 | 55.6 (0.2) | 0.03 (0.02) | 58.9 (0.5) | - | - |
| 9 | 1:0:0:0:1 | - | 379.6 (8.4) | 0.61 (0.03) | 292.1 (71.1) | 2177.8(2282.2) | 3224.3 (2805.0) |
| | | 0.45 | 130.9 (2.8) | 0.15 (0.01) | 157.5 (3.4) | - | - |
| | | 0.22 | 133.5 (7.6) | 0.12 (0.01) | 155.3 (10.7) | - | - |
| 10 | 0:1:1:0:0 | - | 602.9 (299.1) | 0.68 (0.17) | 256.0 (61.3) | 1919.4 (2217.0) | 3540.9 (2979.1) |
| | | 0.45 | 172.96 (36.5) | 0.51 (0.11) | 44.6 (37.2) | 166.8 (32.6) | 175.1 (239.9) |
| | | 0.22 | - | - | - | - | - |
| 11 | 0:1:0:1:0 | - | 725.3 (49.6) | 0.90 (0.08) | 299.3 (31.6) | 498.2 (802.5) | 1723.5 (2882.3) |
| | | 0.45 | 155.1 (1.0) | 0.15 (0.01) | 184.5 (5.2) | - | - |
| | | 0.22 | 125.9 (3.5) | 0.13 (0.01) | 144.4 (2.9) | - | - |
| 12 | 0:1:0:0:1 | - | 768.8 (248.7) | 0.89 (0.13) | 327.9 (151.1) | 1737.7 (3009.7) | - |
| | | 0.45 | 160.5 (3.1) | 0.12 (0.01) | 183.1 (5.8) | - | - |
| | | 0.22 | 145.6 (3.2) | 0.11 (0.00) | 166.0 (4.2) | - | - |
| 13 | 0:0:1:1:0 | - | - | - | - | - | - |
| 14 | 0:0:1:0:1 | - | - | - | - | - | - |
| 15 | 0:0:0:1:1 | - | 770.4 (141.8) | 0.88 (0.10) | 277.1 (26.0) | 1853.3 (3210.1) | - |
| | | 0.45 | 174.0 (2.8) | 0.11 (0.01) | 196.8 (6.9) | - | - |
| | | 0.22 | 160.9 (1.3) | 0.08 (0.01) | 176.8 (1.9) | - | - |
| 16 | 1:1:1:0:0 | - | 244.2 (12.1) | 0.24 (0.00) | 239.7 (19.2) | 3597.3 (3115.4) | - |
| | | 0.45 | 157.1 (9.3) | 0.15 (0.00) | 167.2 (6.6) | 1687.3 (2922.5) | - |
| | | 0.22 | 132.2 (3.9) | 0.13 (0.02) | 144.2 (1.2) | - | - |

| | | | | | | | |
|---|---|---|---|---|---|---|---|
| 17 | 1:1:0:1:0 | - | 692.8 (167.7) | 0.88 (0.08) | 119.6 (199.1) | 137.2 (140.3) | 190.3 (38.0) |
| | | 0.45 | - | - | - | - | - |
| | | 0.22 | - | - | - | - | - |
| 18 | 1:1:0:0:1 | - | 412.5 (25.6) | 0.65 (0.05) | 266.2 (33.3) | 1768 (582.3) | 4796.3 (247.6) |
| | | 0.45 | 135.1 (2.8) | 0.15 (0.01) | 11.8 (20.4) | 160.3 (3.5) | 1494.9 (2556.6) |
| | | 0.22 | 141.4 (6.2) | 0.14 (0.00) | 12.6 (21.8) | 164.7 (5.9) | - |
| 19 | 0:1:1:1:0 | - | 719.7 (42.9) | 0.89 (0.03) | 57.8 (50.1) | 102.5 (176.3) | 195.8 (37.1) |
| | | 0.45 | - | - | - | - | - |
| | | 0.22 | - | - | - | - | - |
| 20 | 1:0:1:1:0 | - | 209.2 (1.6) | 0.49 (0.00) | 43.0 (0.8) | 370.7 (6.4) | - |
| | | 0.45 | 74.5 (7.5) | 0.41 (0.04) | 128.6 (126.1) | 251.2 (172.8) | - |
| | | 0.22 | 46.5 (0.2) | 0.11 (0.00) | 51.4 (0.5) | - | - |
| 21 | 1:0:1:0:1 | - | 541.2 (167.6) | 0.76 (0.10) | 20.4 (33.5) | 175.5 (37.2) | - |
| | | 0.45 | 147.9 (12.9) | 0.34 (0.04) | 5.2 (6.2) | 121.8 (26.5) | - |
| | | 0.22 | 96.8 (13.6) | 0.46 (0.14) | 1.2 (0.2) | 16.7 (22.9) | 116.3 (7.1) |
| 22 | 1:0:01:1 | - | 405.1 (25.2) | 0.64 (0.04) | 317.3 (57.5) | 1463.0 (2534.0) | 3679.8(2358.8) |
| | | 0.45 | 132.4 (1.5) | 0.17 (0.01) | 157.6 (2.4) | 1684.5(2862.7) | - |
| | | 0.22 | 140.4 (3.9) | 0.14 (0.01) | 164.1 (1.9) | 1579.2 (2706.2) | - |
| 23 | 0:1:1:0:1 | - | 1095.8 (750.2) | 0.83 (0.16) | 98.4 (25.9) | 183.6 (55.3) | 379.4 (129.9) |
| | | 0.45 | 143.7 (25.1) | 0.37 (0.03) | 17.5 (22.7) | 118.3 (20.3) | 230.0 (374.3) |
| | | 0.22 | 114.6 (4.1) | 0.33 (0.05) | 1.6 (1.7) | 12.4 (10.1) | 131.7 (14.1) |
| 24 | 0:1:0:1:1 | - | 860.2 (284.0) | 0.91 (0.09) | 122.2 (105.9) | 306.5 (39.7) | 1788.3 (3013.9) |
| | | 0.45 | 155.6 (1.8) | 0.14 (0.00) | 180.5 (6.2) | - | - |
| | | 0.22 | 148.3 (1.3) | 0.11 (0.02) | 165.5 (1.8) | - | - |
| 25 | 0:0:1:1:1 | - | 651.7 (312.3) | 0.81 (0.21) | 193.6 (36.5) | 668.9 (297.6) | 1494.0 (2585.1) |
| | | 0.45 | - | - | - | - | - |
| | | 0.22 | - | - | - | - | - |
| 26 | 1-1-1-1-0 | - | 269.9 (6.3) | 0.18 (0.01) | 294.7 (4.7) | 5015.7 (238.1) | - |
| | | 0.45 | 164.8 (4.8) | 0.09 (0.02) | 179.2 (4.8) | - | - |
| | | 0.22 | 153.7 (1.4) | 0.08 (0.01) | 167.2 (3.2) | - | - |
| 27 | 0-1-1-1-1 | - | 553.6 (68.3) | 0.78 (0.04) | 184.7 (37.0) | 225.6 (105.2) | - |
| | | 0.45 | 159.9 (10.1) | 0.182 (0.03) | 163.4 (9.4) | 1723.4 (2984.9) | - |
| | | 0.22 | 130.7 (3.3) | 0.16 (0.05) | 138.4 (7.9) | - | - |
| 28 | 1-0-1-1-1 | - | 324.9 (30.6) | 0.55 (0.07) | 179.9 (16.2) | 388 (672.0) | 1695.7 (2937.0) |
| | | 0.45 | 145.4 (5.2) | 0.25 (0.02) | 143.8 (10.5) | - | - |
| | | 0.22 | 126.4 (14.2) | 0.23 (0.023) | 141.2 (5.1) | 1724.7 (2969.9) | - |
| 29 | 1-1-0-1-1 | - | 327.5 (17.2) | 0.58 (0.04) | 299.6 (44.2) | 1374.7 (2381.0) | 3612.3 (1691.1) |
| | | 0.45 | 133.0 (2.2) | 0.15 (0.01) | 160.5 (5.6) | - | - |
| | | 0.22 | 136.0 (1.6) | 0.13 (0.00) | 11.9 (20.6) | 160.3 (1.3) | - |
| 30 | 1:1:1:0:1 | - | 472.8 (80.3) | 0.72 (0.08) | 112.1 (122.7) | 158.9 (19.2) | - |
| | | 0.45 | 144.7 (3.7) | 0.18 (0.02) | 149.9 (1.1) | - | - |
| | | 0.22 | 126.3 (1.2) | 0.15 (0.01) | 13.0 (22.5) | 141.8 (3.5) | - |
| 31 | 1:1:1:1:1 | - | 397.1 (105.8) | 0.64 (0.16) | 42.1 (72.9) | 176.5 (25.9) | - |
| | | 0.45 | 146.2 (3.1) | 0.13 (0.01) | 157.3 (3.4) | - | - |
| | | 0.22 | 133.9 (2.4) | 0.12 (0.00) | 148.5 (3.4) | - | - |

1

**Table 6**

Solvent effect on size and polydispersity of $MPC_{100}$-$DPA_{100}$ nanoparticle systems prepared via nanoprecipitation (Mean ± SD, n = 3). See Table 2 for solvent formulation details.

| | Solvent Combination | Filter (μm) | Diameter (*ZAve*) (nm) (±SD) | Polydispersity (Pd) (±SD) | *Dh*[1] (nm) (±SD) | *Dh*[2] (nm) (±SD) | *Dh*[3] (nm) (±SD) |
|---|---|---|---|---|---|---|---|
| 1 | 1:0:0:0:0 | - | 70.3 (0.6) | 0.03 (0.01) | 73.9 (0.7) | - | - |
| | | 0.45 | 69.6 (0.5) | 0.04 (0.01) | 73.4 (0.8) | - | - |
| | | 0.22 | 69.2 (0.2) | 0.03 (0.00) | 72.9 (0.4) | - | - |
| 2 | 0:1:0:0:0 | - | 223.0 (16.7) | 0.38 (0.02) | 278.5 (33.0) | 2047.7 (2391.0) | 3190.3 (2768.2) |
| | | 0.45 | 135.8 (6.4) | 0.17 (0.01) | 161.6 (8.7) | 1579.0 (2734.9) | - |
| | | 0.22 | 153.7 (5.2) | 0.19 (0.01) | 23.2 (20.5) | 191.4 (4.9) | - |
| 3 | 0:0:1:0:0 | - | - | - | - | - | - |
| 4 | 0:0:0:1:0 | - | - | - | - | - | - |
| 5 | 0:0:0:0:1 | - | 437.1 (47.2) | 0.61 (0.03) | 504.4 (70.67 | 1760.3 (3049.0) | 3357.4 (2743.2) |
| | | 0.45 | 137.8 (9.4) | 0.17 (0.01) | 165.1 (12.6) | - | - |
| | | 0.22 | 172.7 (3.9) | 0.16 (0.01) | 204.6 (5.5) | - | - |
| 6 | 1:1:0:0:0 | - | 62.4 (0.7) | 0.05 (0.01) | 66.6 (0.7) | - | - |
| | | 0.45 | 61.3 (0.5) | 0.05 (0.02) | 65.4 (0.3) | - | - |
| | | 0.22 | 61.5 (0.4) | 0.05 (0.01) | 65.7 (0.7) | - | - |
| 7 | 1:0:1:0:0 | - | 559.6 (266.6) | 0.65 (0.22) | 279.3 (86.4) | 3480.7 (2782.1) | - |
| | | 0.45 | 131.0 (26.2) | 0.52 (0.16) | 15.7 (23.2) | 190.3 (12.6) | 1853.9 (3209.6) |
| | | 0.22 | 195.1 (22.4) | 0.28 (0.02) | 224.4 (25.4) | 1733.1 (2972.2) | - |
| 8 | 1:0:0:1:0 | - | 75.8 (0.7) | 0.06 (0.00) | 81.1 (0.6) | - | - |
| | | 0.45 | 74.9 (0.9) | 0.05 (0.02) | 79.8 (0.9) | - | - |
| | | 0.22 | 75.2 (0.5) | 0.04 (0.01) | 79.5 (0.5) | - | - |
| 9 | 1:0:0:0:1 | - | 238.4 (0.6) | 0.35 (0.02) | 14.6 (25.2) | 326.5 (13.8) | 4690.0 (454.0) |
| | | 0.45 | 138.7 (6.3) | 0.18 (0.01) | 21.0 (18.4) | 168.9 (9.8) | - |
| | | 0.22 | 159.3 (6.5) | 0.19 (0.01) | 194.6 (10.6) | 3264.3 (2828.4) | - |
| 10 | 0:1:1:0:0 | - | 309.3 (32.0) | 0.45 (0.05) | 336.8 (56.5) | 574.3 (994.8) | 4781.3 (490.2) |
| | | 0.45 | 172.2 (15.8) | 0.28 (0.04) | 4.9 (6.2) | 22.7 (27.2) | 197.7 (25.1) |
| | | 0.22 | 184.9 (20.5) | 0.23 (0.08) | 0.8 (1.3) | 209.1 (16.9) | 3293.3 (2829.3) |
| 11 | 0:1:0:1:0 | - | 235.0 (10.8) | 0.45 (0.02) | 293.3 (27.0) | 1613.4 (2763.2) | 3846.0 (1377.6) |
| | | 0.45 | 131.5 (6.3) | 0.13 (0.01) | 149.13 (8.50) | - | - |
| | | 0.22 | 152.5 (5.8) | 0.15 (0.01) | 12.8 (22.2) | 178.6 (7.9) | - |
| 12 | 0:1:0:0:1 | - | 523.2 (21.7) | 0.69 (0.02) | 448.1 (146.3) | 1977.6 (2525.2) | 3412.7 (2960.7) |
| | | 0.45 | 164.0 (2.0) | 0.17 (0.01) | 196.4 (4.7) | - | - |
| | | 0.22 | 187.5 (3.9) | 0.18 (0.01) | 227.0 (10.3) | - | - |
| 13 | 0:0:1:1:0 | - | - | - | - | - | - |
| 14 | 0:0:1:0:1 | - | 367.1 (156.9) | 0.52 (0.17) | 255.0 (61.2) | 1710.7 (2962.7) | 1869.5 (2861.0) |
| | | 0.45 | 195.1 (29.8) | 0.42 (0.10) | 0.2 (0.4) | 274.9 (122.5) | 1718.0 (2872.2) |
| | | 0.22 | 119.9 (61.3) | 0.61 (0.34) | 1.9 (2.6) | 27.7 (37.7) | 240.6 (36.4) |
| 15 | 0:0:0:1:1 | - | 347.5 (24.3) | 0.58 (0.05) | 339.6 (19.0) | 4800.7 (958.3) | - |
| | | 0.45 | 133.9 (4.0) | 0.17 (0.01) | 23.1 (20.1) | 160.9 (5.1) | - |
| | | 0.22 | 161.6 (1.1) | 0.15 (0.01) | 187.5 (1.8) | 1628.7 (2820.9) | - |
| 16 | 1:1:1:0:0 | - | 461.8 (32.1) | 0.50 (0.05) | 486.4 (141.7) | 2919.4 (2503.6) | - |
| | | 0.45 | 174.1 (6.4) | 0.15 (0.03) | 15.3 (26.5) | 205.6 (9.5) | - |

| | | | | | | | |
|---|---|---|---|---|---|---|---|
| | | 0.22 | 184.6 (8.8) | 0.16 (0.01) | 213.4 (13.3) | - | - |
| 17 | 1:1:0:1:0 | - | 461.5 (93.7) | 0.58 (0.15) | 334.3 (101.6) | 1442.3 (2422.4) | - |
| | | 0.45 | 170.2 (13.5) | 0.26 (0.04) | 3.2 (5.5) | 191.8 (20.9) | 481.7 (834.3) |
| | | 0.22 | 199.6 (14.3) | 0.21 (0.03) | 221.3 (10.4) | 1572.3 (2723.4) | - |
| 18 | 1:1:0:0:1 | - | 245.2 (13.7) | 0.41 (0.03) | 356.3 (53.8) | 4700.7 (335.8) | - |
| | | 0.45 | 145.3 (5.3) | 0.18 (0.00) | 177.47 (7.5) | - | - |
| | | 0.22 | 163.6 (5.9) | 0.20 (0.01) | 203.2 (8.5) | 2964.3 (2575.8) | - |
| 19 | 0:1:1:1:0 | - | 500.7 (32.5) | 0.62 (0.03) | 58.5 (65.0) | 303.4 (372.2) | 340.4 (7.1) |
| | | 0.45 | 158.7 (3.8) | 0.18 (0.00) | 179.6 (2.8) | 1673.0 (2897.7) | - |
| | | 0.22 | 190.5 (5.2) | 0.16 (0.00) | 220.7 (1.6) | 1604.3 (2778.8) | - |
| 20 | 1:0:1:1:0 | - | 65.5 (2.2) | 0.06 (0.01) | 70.1 (2.9) | - | - |
| | | 0.45 | 64.8 (1.8) | 0.05 (0.02) | 69.30 (1.5) | - | - |
| | | 0.22 | 64.5 (1.5) | 0.06 (0.01) | 69.3 (2.1) | - | - |
| 21 | 1:0:1:0:1 | - | 356.6 (12.3) | 0.42 (0.03) | 27.4 (47.5) | 454.4 (76.0) | 4599.7 (606.4) |
| | | 0.45 | 176.8 (2.2) | 0.12 (0.01) | 200.2 (3.9) | - | - |
| | | 0.22 | 188.0 (7.8) | 0.14 (0.01) | 217.6 (10.8) | - | - |
| 22 | 1:0:01:1 | - | 205.8 (12.5) | 0.39 (0.01) | 10.8 (18.6) | 306.1 (15.2) | 4258.7 (314.5) |
| | | 0.45 | 131.6 (6.0) | 0.16 (0.01) | 156.0 (8.8) | 3194.7 (2779.0) | - |
| | | 0.22 | 147.5 (11.8) | 0.19 (0.02) | 179.5 (19.7) | 3047.3 (2639.1) | - |
| 23 | 0:1:1:0:1 | - | 346.3 (27.6) | 0.50 (0.02) | 93.9 (24.6) | 334.8 (23.9) | 3522.3 (3051.2) |
| | | 0.45 | 158.5 (5.5) | 0.14 (0.01) | 177.3 (9.7) | 1720.3 (2979.7) | - |
| | | 0.22 | 182.1 (5.7) | 0.14 (0.01) | 211.2 (6.6) | - | - |
| 24 | 0:1:0:1:1 | - | 507.8 (68.7) | 0.75 (0.03) | 285.00 (99.5) | 2356.37 (2786.3) | 3664.3 (3174.0) |
| | | 0.45 | 134.0 (7.5) | 0.18 (0.01) | 163.3 (11.8) | - | - |
| | | 0.22 | 156.0 (1.5) | 0.19 (0.01) | 191.5 (6.7) | 1694.3 (2874.9) | - |
| 25 | 0:0:1:1:1 | - | 384.7 (133.9) | 0.59 (0.16) | 252.0 (23.5) | 703.2 (1138.0) | 2483.0 (2637.1) |
| | | 0.45 | 128.5 (37.5) | 0.54 (0.15) | 20.6 (28.2) | 205.0 (32.2) | 3078.1 (2679.9) |
| | | 0.22 | 179.1 (40.8) | 0.28 (0.06) | 218.5 (49.5) | 1798.4 (3113.1) | - |
| 26 | 1-1-1-1-0 | - | 521.3 (43.4) | 0.69 (0.05) | 142.4 (87.8) | 377.0 (44.5) | 2125.0 (2784.9) |
| | | 0.45 | 165.9 (3.4) | 0.13 (0.01) | 191.4 (5.2) | - | - |
| | | 0.22 | 183.7 (11.4) | 0.15 (0.02) | 213.8 (10.5) | - | - |
| 27 | 0-1-1-1-1 | - | 545.2 (7.8) | 0.69 (0.05) | 239.2 (230.0) | 352.5 (31.1) | 462.6 (692.7) |
| | | 0.45 | 167.4 (1.0) | 0.13 (0.00) | 190.0 (5.2) | 1610.0 (2788.6) | - |
| | | 0.22 | 182.9 (9.8) | 0.15 (0.02) | 16.0 (27.7) | 211.3 (10.5) | - |
| 28 | 1-0-1-1-1 | - | 506.5 (31.3) | 0.65 (0.05) | 47.2 (41.4) | 312.0 (49.7) | 437.6 (419.6) |
| | | 0.45 | 173.0 (3.6) | 0.14 (0.00) | 199.9 (4.7) | - | - |
| | | 0.22 | 189.4 (8.7) | 0.15 (0.01) | 222.4 (12.7) | - | - |
| 29 | 1-1-0-1-1 | - | 242.5 (6.5) | 0.43 (0.03) | 13.1 (22.7) | 370.7 (43.0) | 4293.3 (192.0) |
| | | 0.45 | 136.9 (5.4) | 0.16 (0.01) | 162.9 (7.7) | - | - |
| | | 0.22 | 153.03 (9.1) | 0.19 (0.03) | 187.5 (13.7) | 3147.6 (2708.8) | - |
| 30 | 1:1:1:0:1 | - | 533.4 (78.5) | 0.65 (0.10) | 20.9 (36.2) | 502.8 (77.9) | 1657.4 (2627.3) |
| | | 0.45 | 168.4 (4.5) | 0.14 (0.01) | 194.3 (7.4) | - | - |
| | | 0.22 | 188.0 (10.0) | 0.15 (0.02) | 221.0 (5.8) | - | - |
| 31 | 1:1:1:1:1 | - | 586.8 (79.6) | 0.74 (0.09) | 289.4 (98.9) | 612.2 (702.6) | 1889.0 (2431.2) |
| | | 0.45 | 154.7 (15.0) | 0.14 (0.01) | 12.9 (22.3) | 179.4 (18.5) | - |
| | | 0.22 | 188.6 (7.0) | 0.15 (0.03) | 221.0 (5.6) | - | - |

**Table 7**

AFM measurements and roughness parameters (R) of MPC-DPA copolymer film surface roughness (Mean ± SD, n = 6). Where Rq = root mean square roughness; Ra = average roughness; and Rz = ten point average roughness. See Table 2 for solvent formulation details.

| # | $MPC_{30}$ - $DPA_{100}$ | Rq (nm) | Ra (nm) | Rz (nm) |
|---|---|---|---|---|
| **(a)** | Solvent 15 | 231.5 (100.0) | 183.6 (86.8) | 867.3 (301.1) |
| **(b)** | Solvent 24 | 296.4 (72.0) | 242.4 (61.0) | 1167.0 (172.7) |
| **(c)** | Solvent 26 | 12.9 (2.3) | 10.2 (1.8) | 81.9 (6.3) |
| | $MPC_{100}$ - $DPA_{100}$ | **Rq (nm)** | **Ra (nm)** | **Rz (nm)** |
| **(d)** | Solvent 12 | 80.0 (4.6) | 61.1 (3.3) | 529.1 (48.0) |
| **(e)** | Solvent 16 | 16.5 (1.7) | 13.0 (1.6) | 72.7 (5.9) |
| **(f)** | Solvent 29 | 70.7 (16.6) | 52.9 (10.0) | 284.1 (43.3) |

**Table 8**

Solvent effect on size and polydispersity of MPC-DPA nanoparticle systems prepared via film-rehydration (Mean ± SD, n = 3). See Table 2 for solvent formulation details.

**$MPC_{30}$ - $DPA_{100}$**

| Solvent Combination | | Filter (µm) | Diameter (*ZAve*) (nm) (±SD) | Polydispersity (Pd) (±SD) | *Dh*[1] (nm) (±SD) | *Dh*[2] (nm) (±SD) | *Dh*[3] (nm) (±SD) |
|---|---|---|---|---|---|---|---|
| 15 | 0:0:0:1:1 | - | 2257.0 (743.8) | 0.70 (0.28) | 645.9 (508.9) | 2024.0 (3062.5) | 2788.4 (2224.6) |
| | | 0.45 | 151.4 (3.1) | 0.22 (0.04) | 169.2 (8.0) | 4644.3 (570.5) | - |
| | | 0.22 | 139.1 (9.1) | 0.17 (0.04) | 160.3 (8.3) | - | - |
| 24 | 0:1:0:1:1 | - | 3026.0 (1015.3) | 0.48 (0.40) | 308.9 (365.0) | 1023.4 (493.5) | 2587.5 (2243.2) |
| | | 0.45 | 149.2 (9.2) | 0.20 (0.01) | 165.2 (19.4) | 1662.0 (2878.6) | 3368.7 (1296.7) |
| | | 0.22 | 142.8 (7.8) | 0.18 (0.00) | 163.6 (5.7) | 1768.3 (3062.9) | - |
| 26 | 1:1:1:1:0 | - | 2871.3 (844.6) | 0.59 (0.30) | 1688.5 (1250.5) | 1763.9 (2514.3) | 2130.6 (2509.9) |
| | | 0.45 | 144.7 (9.9) | 0.20 (0.03) | 162.2 (11.5) | 4427.0 (797.9) | - |
| | | 0.22 | 139.3 (2.5) | 0.18 (0.03) | 160.1 (3.4) | 1741.0 (3015.5) | 3190.4 (2734.6) |

**$MPC_{100}$ - $DPA_{100}$**

| Solvent Combination | | Filter (µm) | Diameter (*ZAve*) (nm) (±SD) | Polydispersity (Pd) (±SD) | *Dh*[1] (nm) (±SD) | *Dh*[2] (nm) (±SD) | *Dh*[3] (nm) (±SD) |
|---|---|---|---|---|---|---|---|
| 12 | 0:1:0:0:1 | - | 831.3 (343.2) | 0.79 (0.27) | 164.9 (144.3) | 920.3 (437.2) | 4609.7 (29.0) |
| | | 0.45 | 126.7 (16.4) | 0.16 (0.04) | 150.3 (12.9) | 1525.7 (2642.5) | - |
| | | 0.22 | 153.8 (10.8) | 0.14 (0.00) | 178.5 (11.1) | - | - |
| 16 | 1:1:1:0:0 | - | 552.2 (318.7) | 0.78 (0.04) | 288.1 (265.9) | 1723.3 (1981.3) | 1851.3 (2441.2) |
| | | 0.45 | 118.6 (6.1) | 0.10 (0.03) | 134.1 (11.4) | - | - |
| | | 0.22 | 136.6 (14.8) | 0.13 (0.00) | 155.9 (16.6) | - | - |
| 29 | 1:1:0:1:1 | - | 574.0 (414.4) | 0.69 (0.25) | 302.8 (147.7) | 2291.7 (1608.9) | 2557.0 (2327.8) |
| | | 0.45 | 124.4 (14.4) | 0.12 (0.03) | 141.2 (16.2) | - | - |
| | | 0.22 | 148.3 (23.1) | 0.12 (0.02) | 168.5 (24.5) | 1648.3 (2855.0) | - |

**Table 9**

MPC-DPA nanoparticle size, polydispersity, zeta potential, and curcumin loading via nanoprecipitation. (Mean ± SD, n=3). See Table 2 for solvent formulation details.

| **Formulation 26 $MPC_{30}$-$DPA_{100}$** | **Parameters values after filtration (0.22µm): Mean ± SD, n=3** | | | | | |
|---|---|---|---|---|---|---|
| | Diameter (nm) | Poly dispersity (Pd) | Zeta Potential (mV) | Encapsulation Efficiency (%) | Loading Capacity (%) | Curcumin Loading (µg $ml^{-1}$) |
| Before loading with curcumin | 153.7 (1.4) | 0.08 (0.01) | -0.34 (1.10) | - | - | - |
| After loading with Curcumin[a] | 141.9 (10.4) | 0.10 (0.01) | -0.83 (0.97) | - | - | - |
| After coating with TMC polymer[b] | 136.4 (3.7) | 0.12 (0.02) | 2.20 (0.09) | - | - | - |
| **Formulation 12 $MPC_{100}$-$DPA_{100}$** | | | | | | |
| Before loading with curcumin | 187.5 (3.9) | 0.18 (0.01) | -0.50 (0.14) | - | - | - |
| After loading with Curcumin[c] | 175.2 (8.1) | 0.18 (0.00) | -0.55 (0.27) | 2.63 (0.30) | 0.22 (0.02) | 0.92 (0.10) |
| After coating with TMC polymer[b] | 162.4 (1.9) | 0.16 (0.00) | -0.31 (0.49) | 2.44 (0.19) | 0.20 (0.01) | 0.85 (0.06) |

**Table 10**

MPC-DPA nanoparticle size, polydispersity, zeta potential, and curcumin loading via film rehydration. (Mean ± SD, n=3). See Table 2 for solvent formulation details.

| **Formulation 26 $MPC_{30}$-$DPA_{100}$** | **Parameters values after filtration (0.22µm): Mean ± SD, n=3** | | | | | |
|---|---|---|---|---|---|---|
| | Diameter (nm) | Poly dispersity (Pd) | Zeta Potential (mV) | Encapsulation Efficiency (%) | Loading Capacity (%) | Curcumin Loading (µg $ml^{-1}$) |
| Before loading with curcumin | 139.3 (2.5) | 0.18 (0.03) | -0.56 (1.74) | - | - | - |
| After loading with Curcumin[a] | 152.5 (30.1) | 0.34 (0.15) | -1.51 (0.11) | - | - | - |
| After coating with TMC polymer[b] | 131.5 (11.6) | 0.23 (0.01) | 7.99 (3.15) | - | - | - |
| **Formulation 12 $MPC_{100}$-$DPA_{100}$** | | | | | | |
| Before loading with curcumin | 153.8 (10.8) | 0.14 (0.00) | -0.33 (0.20) | - | - | - |
| After loading with Curcumin[c] | 163.7 (3.1) | 0.19 (0.01) | -0.83 (0.37) | 1.96 (1.21) | 1.35 (0.83) | 6.86 (4.24) |
| After coating with TMC polymer[b] | 156.8 (6.3) | 0.17 (0.01) | 1.04 (0.72) | 12.19 (4.90) | 8.39 (3.37) | 42.57 (17.12) |

**Figures**

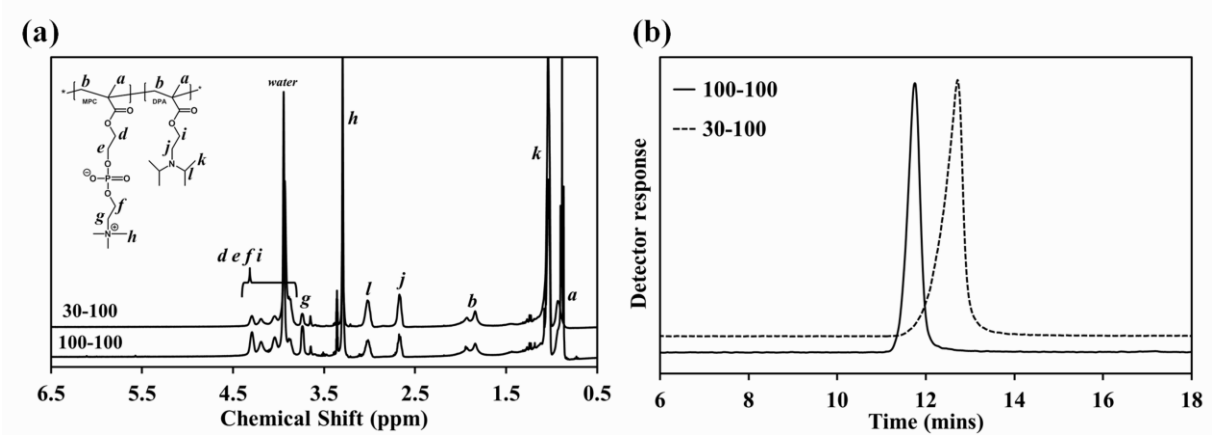


**Fig. 1.** (a) $^{1}$H NMR spectra of $MPC_{30}$-$DPA_{100}$ and $MPC_{100}$-$DPA_{100}$ diblock copolymers. (b) GPC elution profiles of $MPC_{30}$-$DPA_{100}$ and $MPC_{100}$-$DPA_{100}$ diblock copolymers.

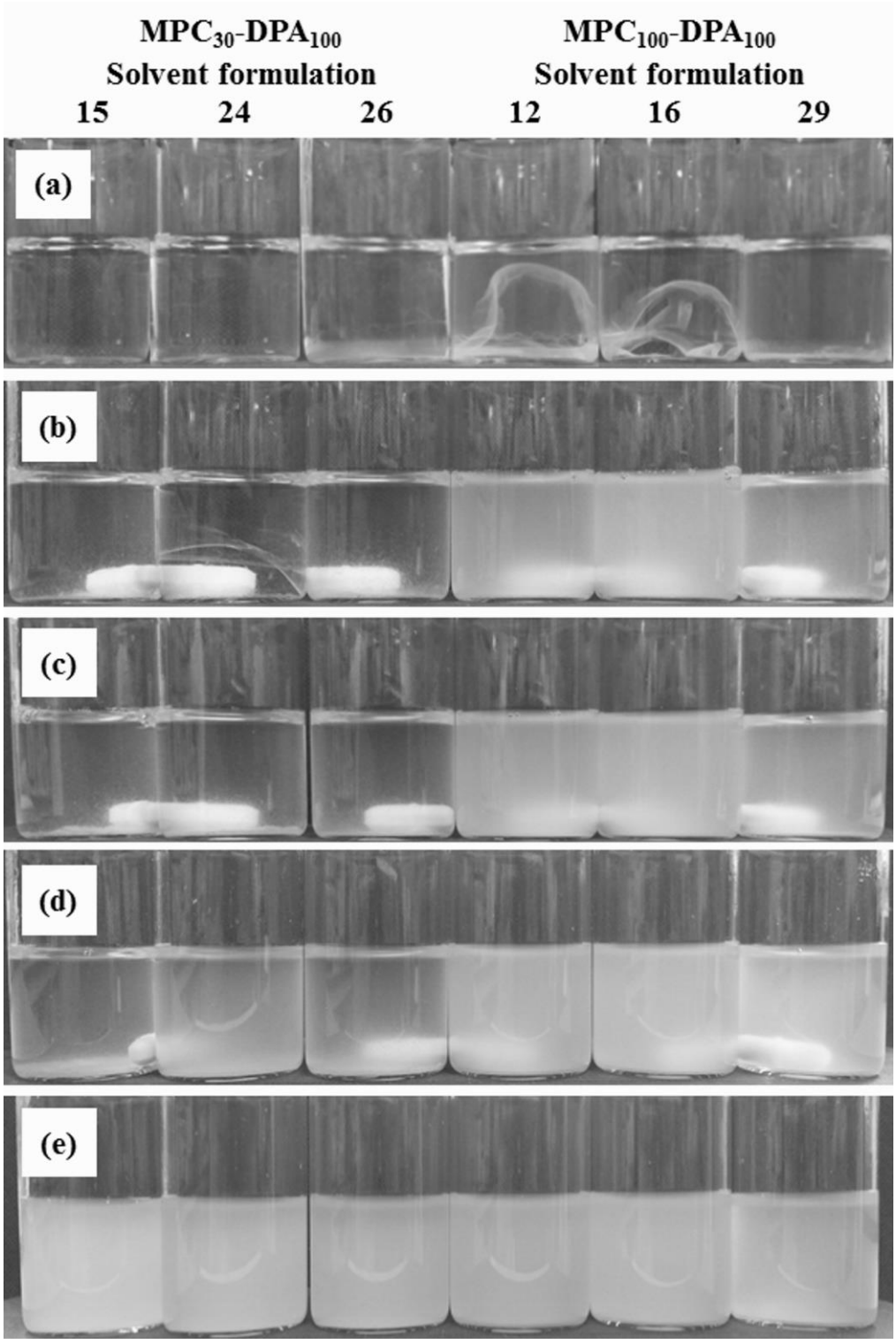


**Fig. 2.** Film rehydration of MPC-DPA copolymers at (a) t = 0, (b) t = 1 day, (c) t = 2 days, (d) t = 4 days, (e) t = 7 days. See Table 2 for solvent formulation details.

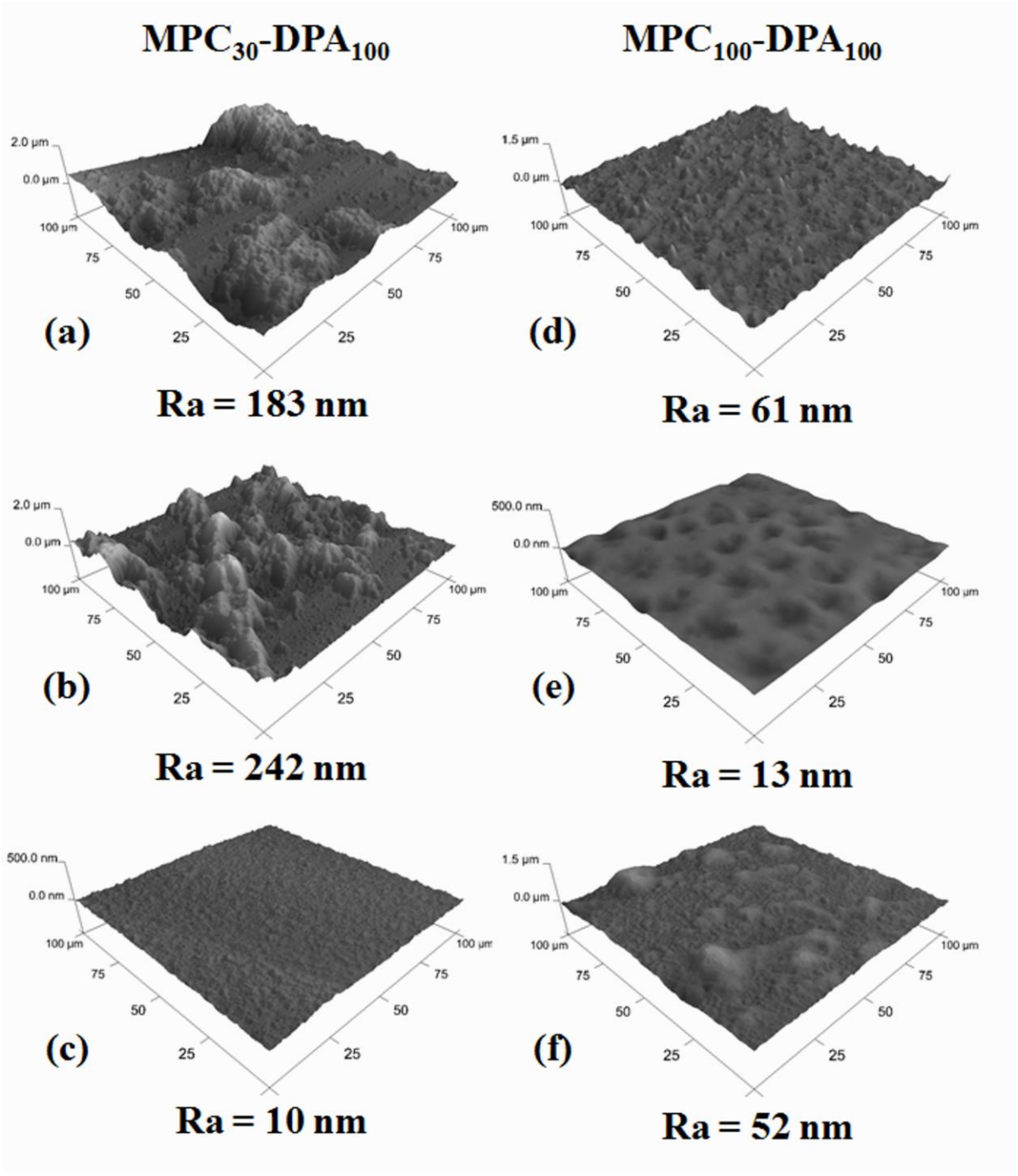


**Fig. 3.** Representative AFM images of MPC-DPA copolymer film surface topography; where Ra = average roughness, for solvent combinations 15(a), 24(b), 26(c), 12(d), 16(e), and 29(f). See Table 2 for solvent formulation details.

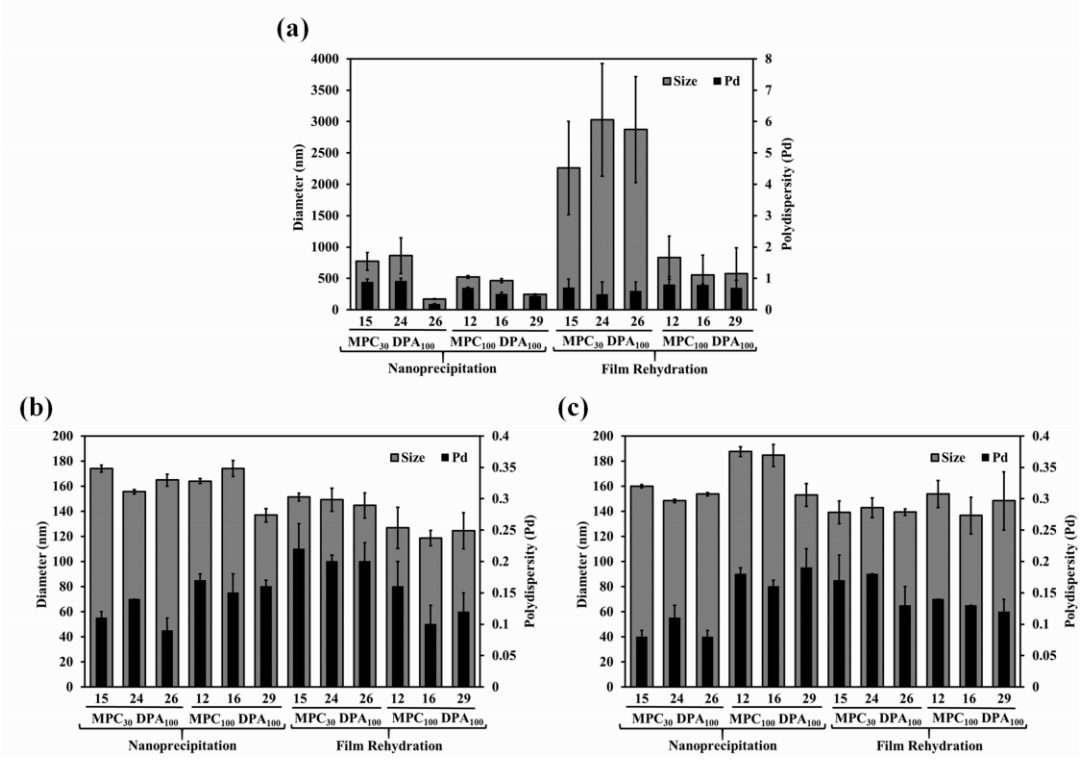


**Fig. 4.** Comparison of preparation method, nanoprecipitation vs film-rehydration, effects on the particle size and polydispersity of MPC-DPA nanosystems measured using DLS (a) without filtration, (b) after filtration (0.45µm), and (c) after filtration (0.22µm). (Mean ± SD, n=3). See Table 2 for solvent formulation details.

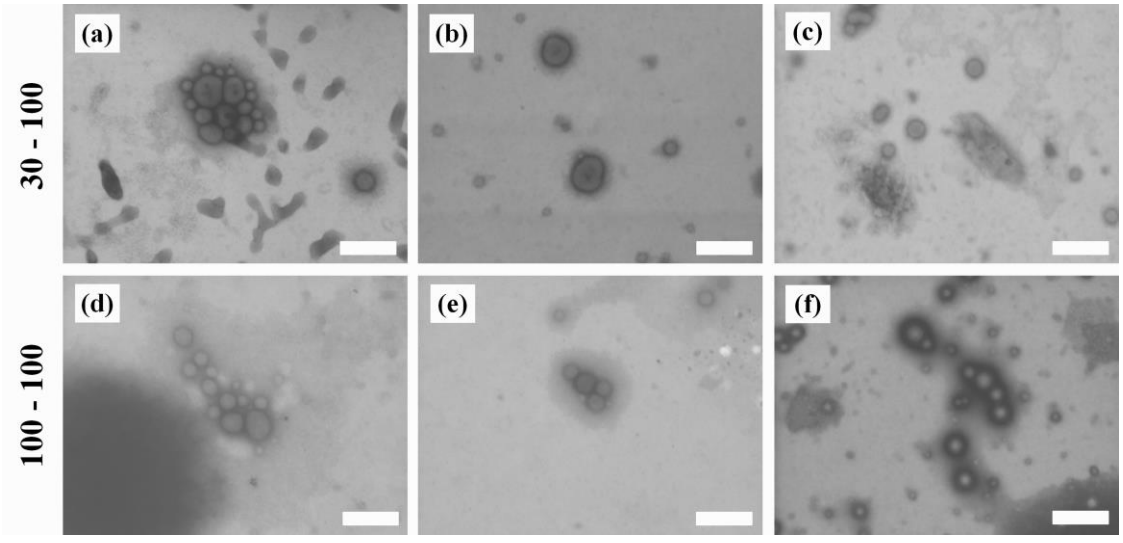


**Fig. 5.** Scanning transmission electron microscopy (STEM) images of $MPC_{30}$-$DPA_{100}$ (a, b, c) and $MPC_{100}$-$DPA_{100}$ (d, e, f) nanoparticles formed via nanoprecipitation from solvent formulations 15 (a), 24 (b), 26 (c), 12 (d), 16 (e), and 29 (f), as per Table 2. Scale bar = 200 nm. See Table 2 for solvent formulation details.

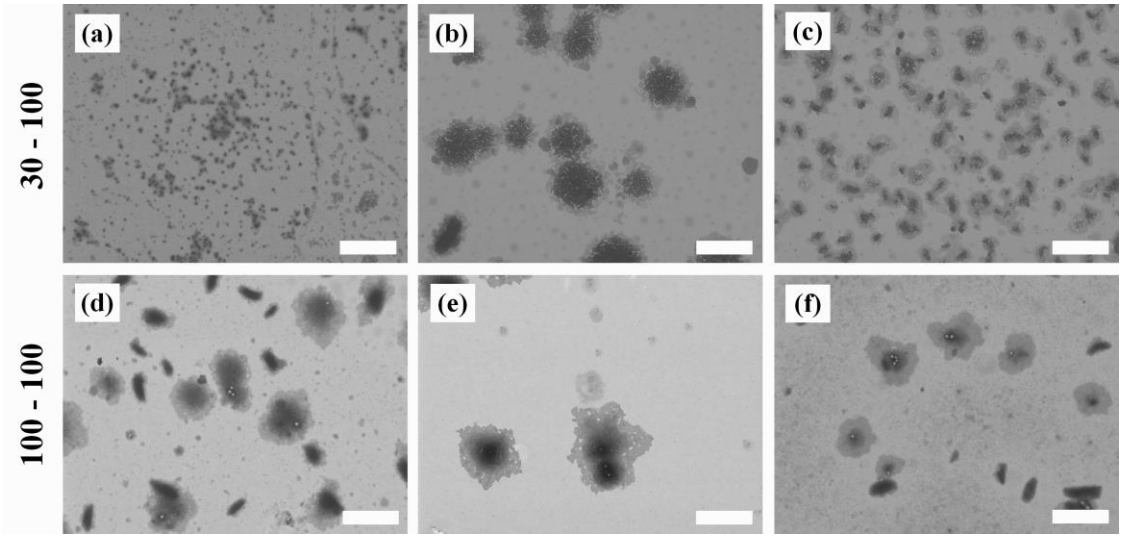


**Fig. 6.** Scanning transmission electron microscopy (STEM) images of $MPC_{30}$-$DPA_{100}$ (a, b, c) and $MPC_{100}$-$DPA_{100}$ (d, e, f) nanoparticles formed via film rehydration cast from solvent formulations 15 (a), 24 (b), 26 (c), 12 (d), 16 (e), and 29 (f), as per Table 2. Scale bar = 800 nm. See Table 2 for solvent formulation details.

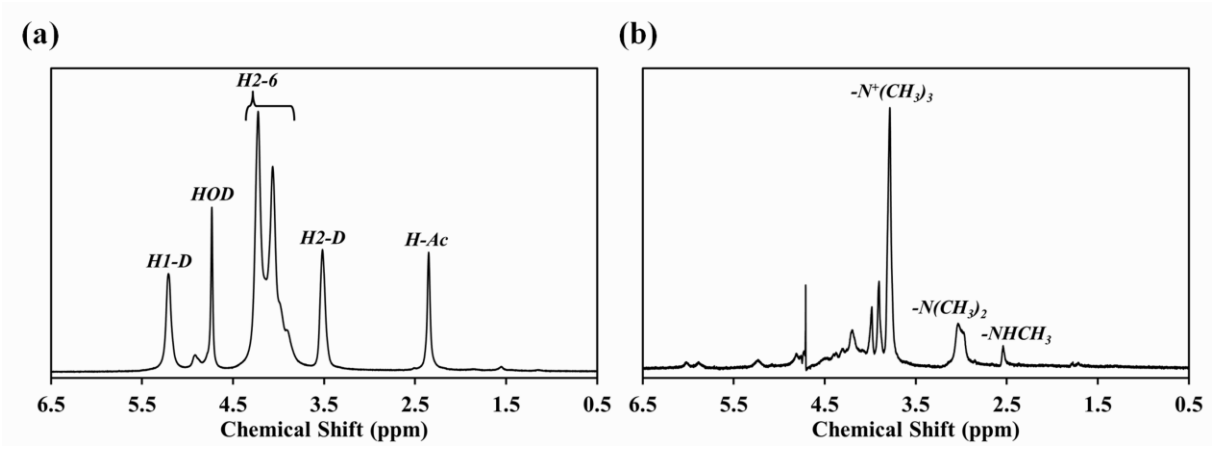


**Fig. 7.** $^{1}H$ NMR spectra of (a) chitosan; chemical shift (ppm) peak assignments: H-Ac = 2.35, H2-D = 3.52, H2-6 = 3.92 – 4.23, and H1-D = 5.21. NMR solvent peak: HOD = 4.73. (b) TMC; chemical shift (ppm) peak assignments: $-NHCH_3$ = 2.55, $-N(CH_3)_2$ = 3.05, and $-N^{+}(CH_3)_3$ = 3.80.

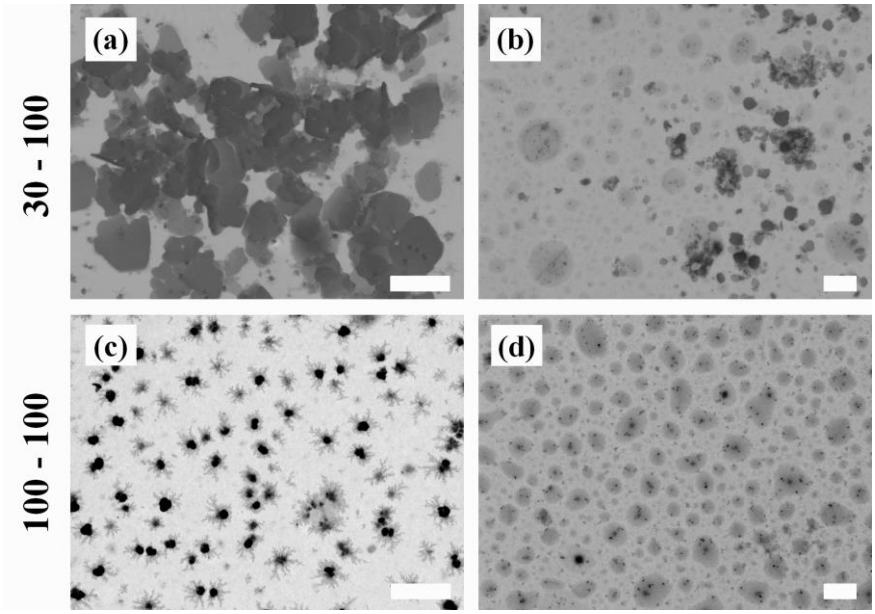


**Fig. 8.** Scanning transmission electron microscopy (STEM) images of $MPC_{30}$-$DPA_{100}$ (a, b) and $MPC_{100}$-$DPA_{100}$ (c, d) nanoparticles formed via nanoprecipitation from solvent formulations 26 (a, b) and 12 (c, d), as per Table 2, and curcumin loaded (a, c) and TMC coated (b, d). Scale bar = 300 nm. See Table 2 for solvent formulation details.

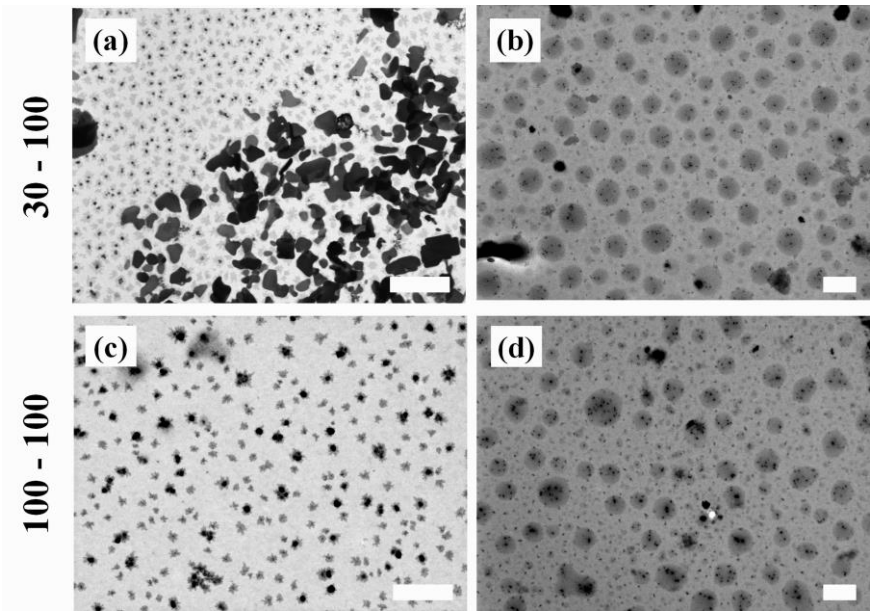


**Fig. 9.** Scanning transmission electron microscopy (STEM) images of $MPC_{30}$-$DPA_{100}$ (a, b) and $MPC_{100}$-$DPA_{100}$ (c, d) nanoparticles formed via film rehydration cast from solvent formulations 26 (a, b) and 12 (c, d), as per Table 2, and curcumin loaded (a, c) and TMC coated (b, d). Scale bar = 300 nm. See Table 2 for solvent formulation details.

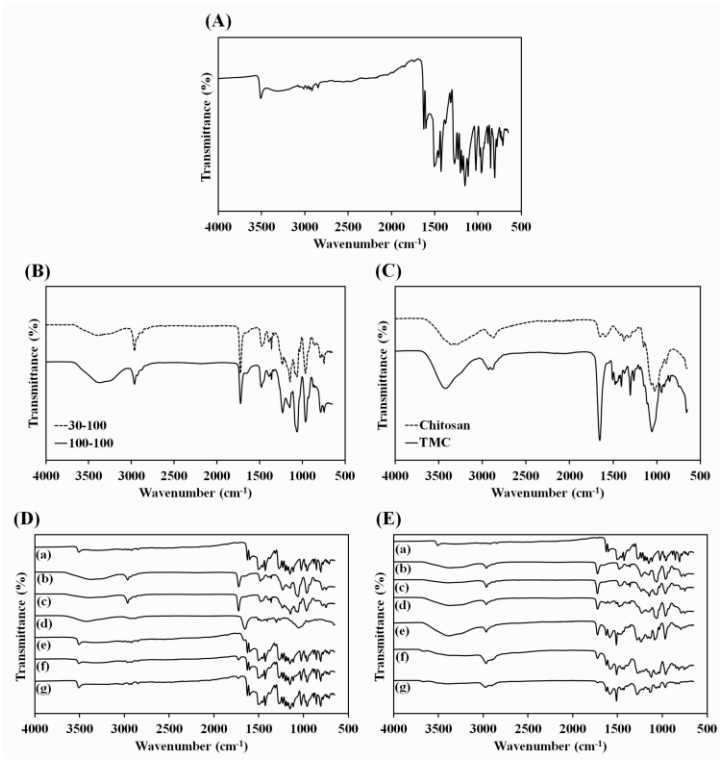


**Fig. 10.** FTIR spectra of **(10a)** curcumin, **(10b)** $MPC_{30}$ -$DPA_{100}$ and $MPC_{100}$ -$DPA_{100}$, **(10c)** chitosan and TMC, **(10d)** curcumin (i), $MPC_{100}$-$DPA_{100}$ (ii), $MPC_{30}$-$DPA_{100}$ (iii), TMC (iv), physical mix of curcumin and TMC (v), physical mix of curcumin and $MPC_{100}$-$DPA_{100}$ (vi), physical mix of curcumin and $MPC_{30}$-$DPA_{100}$ (vii) and **(10e)** pure curcumin (i), $MPC_{100}$-$DPA_{100}$ (ii), $MPC_{30}$-$DPA_{100}$ (iii), solvent mix of curcumin with $MPC_{100}$-$DPA_{100}$ from formulation 12 (iv and v), and solvent mix of curcumin with $MPC_{30}$-$DPA_{100}$ from formulation 26 (vi and vii). The organic solutions for **10e** (iv and vi) were those used for nanoprecipitation, and **10e** (v and vii) for film rehydration.